ISSN: 2376-2136 (Print)
ISSN: 2376-2144 (Online)

# Trends in Renewable Energy

Volume 8, Issue 2, December 2022

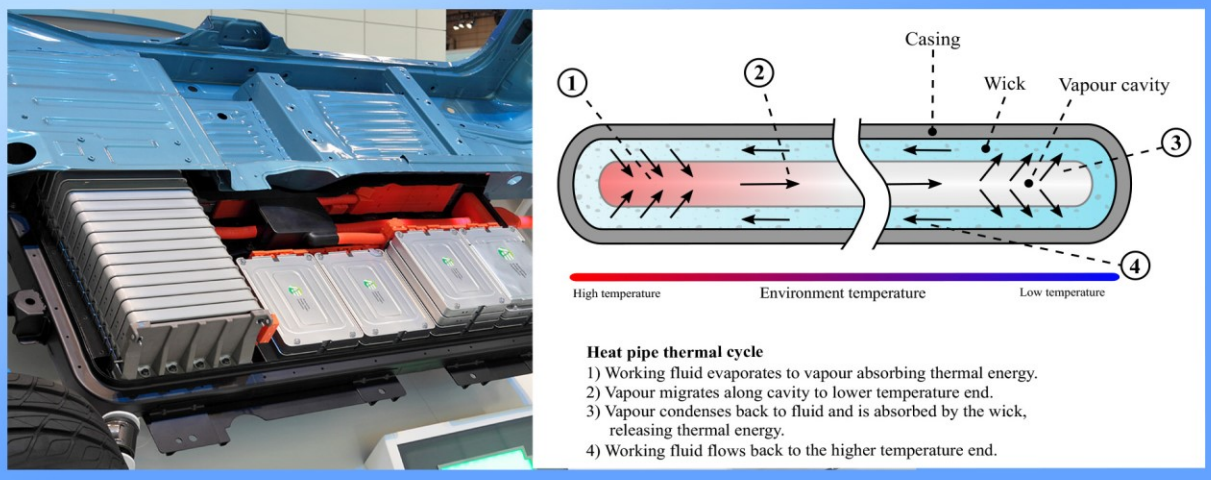


Cover image: Application and Research Progress of Heat Pipe in Thermal Management of Lithium-Ion Battery, see article by Ning et al. in this issue.

ISSN 2376-2136 21
9 772376 213001

futureenergysp.com
thefutureenergy.org

# Trends in Renewable Energy

**ISSN: 2376-2136 (Print) ISSN: 2376-2144 (Online)**

**http://futureenergysp.com/**

---

Trends in Renewable Energy is an open accessed, peer-reviewed semi-annual journal publishing reviews and research papers in the field of renewable energy technology and science.

The aim of this journal is to provide a communication platform that is run exclusively by scientists working in the renewable energy field. Scope of the journal covers: Bioenergy, Biofuel, Biomass, Bioprocessing, Biorefinery, Biological waste treatment, Catalysis for energy generation, Energy conservation, Energy delivery, Energy resources, Energy storage, Energy transformation, Environmental impact, Feedstock utilization, Future energy development, Green chemistry, Green energy, Microbial products, Physico-chemical process for Biomass, Policy, Pollution, Renewable energy, Smart grid, Thermo-chemical processes for biomass, etc.

The Trends in Renewable Energy publishes the following article types: peer-reviewed reviews, mini-reviews, technical notes, short-form research papers, and original research papers.

*The article processing charge (APC), also known as a publication fee, is fully waived for the Trends in Renewable Energy.*

# Editorial Team of Trends in Renewable Energy

| | |
|---|---|
| Dr. Elena Lucchi | Politecnico di Milano, Italy |
| Dr. Muhammad Mujtaba Asad | Faculty of Technical and Vocational Education, Universiti Tun Hussein Onn Malaysia, Malaysia |
| Dr. Afzal Sikander | Department of Instrumentation and Control Engineering, Dr. B. R. Ambedkar National Institute of Technology, India |
| Dr. Padmanabh Thakur | Professor and Head, Department of Electrical Engineering, Graphic Era University, India |
| Dr. K. DHAYALINI | Professor, Department of Electrical and Electronics Engineering, K. Ramakrishnan College of Engineering, Tamilnadu, India |
| Shangxian Xie | Texas A&M University, United States |
| Dr. Tanmoy Dutta | Sandia National Laboratories, United States |
| Dr. Efstathios Stefos | Pontifical Catholic University of Ecuador, Faculty of Exact and Natural Sciences, School of Physical Sciences and Mathematics, Ecuador |
| Dr. Xin Wang | Miami University, United States |
| Dr. Rami El-Emam | Assist. Prof., Faculty of Engineering, Mansoura University, Egypt |
| Dr. Rameshprabu Ramaraj | School of Renewable Energy, Maejo University, Thailand |
| Dr. ZAFER ÖMER ÖZDEMİR | Kirklareli University, Technology Faculty, Turkey |
| Dr. Vijay Yeul | Chandrapur Super Thermal Power Station, India |
| Dr. Mohanakrishna Gunda | VITO - Flemish Institute for Technological Research, Belgium |
| Dr. Shuai Tan | Georgia Institute of Technology, United States |
| Shahabaldin Rezania | Universiti Teknologi Malaysia (UTM), Malaysia |
| Dr. Madhu Sabnis | Contek Solutions LLC, Texas, United States |
| Dr. Qiangu Yan | Mississippi State University, United States |
| Dr. Mustafa Tolga BALTA | Associate Prof., Department of Mechanical Engineering, Faculty of Engineering, Aksaray University, Turkey |
| Dr. María González Alriols | Associate Prof., Chemical and Environmental Engineering Department, University of the Basque Country, Spain |
| Dr. Nattaporn Chaiyat | Assist. Prof., School of Renewable Energy, Maejo University, Thailand |
| Dr. Nguyen Duc Luong | Institute of Environmental Science and Engineering, National University of Civil Engineering, Vietnam |
| Mohd Lias Bin Kamal | Faculty of Applied Science, Universiti Teknologi MARA, Malaysia |
| Dr. N.L. Panwar | Assistant Prof., Department of Renewable Energy Engineering, College of Technology and Engineering, Maharana Pratap University of Agriculture and Technology, India |
| Dr. Caio Fortes | BASF, Brazil |
| Dr. Flavio Prattico | Department of Methods and Models for Economics, Territory and Finance, Sapienza University of Rome, Italy |
| Dr. Wennan ZHANG | Docent (Associate Prof.) and Senior Lecturer in Energy Engineering, Mid Sweden University, Sweden |
| Dr. Ing. Stamatis S. Kalligeros | Associate Prof., Hellenic Naval Academy, Greece |
| Carlos Rolz | Director of the Biochemical Engineering Center, Research Institute at Universidad del Valle, Guatemala |
| Ms. Lilias Makashini | Copperbelt University, Zambia |
| Dr. Ali Mostafaeipour | Assistant Prof., Industrial Engineering Department, Yazd University, Iran |
| Dr. Camila da Silva | Prof., Maringá State University, Brazil |
| Dr. Anna Skorek-Osikowska | Silesian University of Technology, Poland |
| Dr. Shek Atiqure Rahman | Sustainable and Renewable Energy Engineering, College of Engineering, University of Sharjah, Bangladesh |
| Dr. Emad J Elnajjar | Associate Prof., Department of Mechanical Engineering, United Arab Emirates University, United Arab Emirates |
| Dr. Seyed Soheil Mousavi Ajarostaghi | Babol Noshirvani University of Technology, Babol, Iran |
| Dr. Dinesh K. Sharma | National Ecology and Environment Foundation, India |
| Dr. Lakshmana Kumar Ramasamy | Department of Corporate relations, Hindusthan College of Engineering and Technology, India |
| Dr. S. Venkata Ramana | SUSU/National Research University, Russian Federation |
| Dr. Priyanka Marathey | Department of Solar Energy, Pandit Deendayal Petroleum University, India |
| Osamah Siddiqui | University of Ontario Institute of Technology, Canada |

| | |
|---|---|
| Dr. Rupendra Kumar Pachauri | Assistant Prof., Electrical and Electronics Engineering Department, University of Petroleum and Energy Studies, India |
| Dr. Jun Mei | School of Chemistry and Physics, Science and Engineering Faculty, Queensland University of Technology, Australia |
| Dr. Valeria Di Sarli | Institute for Research on Combustion, National Research Council of Italy, Italy |
| Dr. Utkucan Şahin | Assistant Prof., Department of Energy Systems Engineering, Faculty of Technology, Muğla Sıtkı Koçman University, Turkey |
| Dr. ALIASHIM ALBANI | School of Ocean Engineering, Universiti Malaysia Terengganu, Malaysia |
| Dr. Ashwini Kumar | Assistant Prof., College of Engineering, HSBPVT's Parikrama Group of Institutions, India |
| Dr. Hasan AYDOGAN | Associate Prof., Mechanical Engineering Department, Selcuk University, Turkey |
| Dr. Jiekang Wu | Professor, School of Automation, Guangdong University of Technology, China |
| Dr. Ong Huei Ruey | DRB-HICOM University of Automotive, Malaysia |
| Dr. Miguel Ángel Reyes Belmonte | IMDEA Energy Institute, Spain |
| Dr. Chitra Venugopal | Associate Professor in Electrical Engineering, University of Trinidad and Tobago, Trinidad |
| Dr. Amit Kumar Singh | Assistant Prof., Instrumentation & Control Engineering Department, Dr. B.R.A. National Institute of Technology, India |
| Dr. Suvanjan Bhattacharyya | University of Pretoria, South Africa |
| Dr. Karunesh Tiwari | Babu Banarasi Das University, India |
| Dr. Sharadrao A. Vhanalkar | Karmaveer Hire Arts, Science, Commerce and Education College, India |
| Dr. Prasenjit Chatterjee | Assistant Prof. and Head, MCKV Institute of Engineering, India |
| Dr. S. Balamurugan | Mindnotix Technologies, India |
| Dr. Mohammad Nurunnabi | University of Oxford, United Kingdom |
| Dr. Kenneth Okedu | Caledonian College of Engineering, Oman |
| Dr. Cheng Zhang | Sr. Materials Engineer, Medtronic, Inc., United States |
| Dr. Chandani Sharma | Assistant Prof., Department of Electrical Engineering, Graphic Era University, India |
| Dr. Kashif Irshad | Assistant Prof., Mechanical Engineering Department, King Khalid University, Saudi Arabia |
| Dr. Abhijit Bhagavatula | Principal Lead Engineer, Southern Company Services, United States |
| Dr. S. Sathish | Associate Prof., Department of Mechanical Engineering, Hindustan University, India |
| Mr. A. Avinash | Assistant Prof., KPR Institute of Engineering & Technology, India |
| Dr. Bindeshwar Singh | Assistant Prof., Kamla Nehru Institute of Technology, India |
| Dr. Yashar Hashemi | Tehran Regional Electric Company, Iran |
| Dr. Navanietha Krishnaraj R | South Dakota School of Mines and Technology, United States |
| Dr. SANDEEP GUPTA | JECRC University, India |
| Dr. Shwetank Avikal | Graphic Era Hill University, India |
| Dr. Xianglin Zhai | Poochon Scientific LLC, United States |
| Dr. Rui Li | Associate Prof., College of Engineering, China Agricultural University, China |
| Dr. Adam Elhag Ahmed | National Nutrition Policy Chair, Department of Community Services, College of Applied Medical Sciences, King Saud University, Saudi Arabia |
| Dr. Jingbo Li | Massachusetts Institute of Technology, United States |
| Dr. Srikanth Mutnuri | Associate Prof., Department of Biological Sciences, Associate Dean for International Programmes and Collaboration, Birla Institute of Technology & Science, India |
| Dr. Bashar Malkawi | Global Professor of Practice in Law, James E. Rogers College of Law, University of Arizona, United States |
| Dr. Simona Silvia Merola | Istituto Motori - National Research Council of Naples, Italy |
| Dr. Hakan Caliskan | Faculty of Engineering, Department of Mechanical Engineering, Usak University, Turkey |
| Dr. Umashankar Subramaniam | Associate Prof., College of Engineering, Prince Sultan University, Saudi Arabia |
| Dr. Tayfun GÜNDOĞDU | Faculty of Electrical and Electronic Engineering, Department of Electrical Engineering, Istanbul Technical University, Turkey |
| Dr. Yukesh Kannah R | Department of Civil Engineering, Anna University Regional Campus, India |

# Table of Contents

## Volume 8, Issue 2, December 2022

Trends in Renewable Energy
OPEN ACCESS ISSN: 2376-2144
Peer-Reviewed Article futureenergysp.com/index.php/tre

# Construction of Hydrogen Safety Evaluation Model Based on Analytic Hierarchy Process (AHP)

Jianlun Xu, * Minghao Wang, Ping Guo

*School of Mechanical Engineering/Institute of Vehicles and New Energy Technology, North China University of Water Resources and Electric Power, Zhengzhou City, Henan, China*

Received February 23, 2022; Accepted March 11, 2022; Published March 23, 2022

With the large consumption of traditional primary energy, hydrogen as a clean and renewable energy has been widely studied by scholars around the world. Hydrogen is mainly used in hydrogen internal combustion engine and hydrogen fuel cell. Hydrogen internal combustion engine is the direct combustion of hydrogen as fuel, with the advantages of easy use. Alternatively, hydrogen fuel cell converts the chemical energy of hydrogen into electrical energy by electrochemical reaction, which has the advantages of high efficiency and zero pollution. Regardless of the use method, the safety of hydrogen use needs to be considered. However, in the whole life cycle of hydrogen, the process from hydrogen production to the use of hydrogen in automobiles is extremely complex. There are many factors affecting the safety of hydrogen use, and a single factor cannot be used as an evaluation. In order to make the evaluation of hydrogen safety more complete and accurate, the weight of four primary evaluation indexes and eight secondary evaluation indexes affecting hydrogen safety is determined by analytic hierarchy process, and a reliable hydrogen safety evaluation model is established.

*Keywords: Analytic Hierarchy Process (AHP); Multi-objective evaluation; Hydrogen safety grade; Hydrogen fuel cell; Alternative energy sources*

## Introduction

Since the second industrial revolution, the emergence of internal combustion engines has accelerated the global industrial development. Various chemical energy sources have been consumed in large quantities. Oil, coal and natural gas are called the three major energy sources. These three energy sources are all non-renewable primary energy sources. Consumption in the long past can eventually lead to energy shortages. Various renewable clean energy sources have been widely studied as alternative energy sources, in which wind and solar energy account for a large proportion. Solar and wind energy are generally used for photovoltaic power generation and wind power generation，respectively. According to the results released by the World Energy Statistical Yearbook in 2019 [1], the solar and wind energy consumption in the seven regions of the world has increased compared with previous years. The solar and wind energy consumption in the Asia-Pacific region is the highest, reaching 225.4 million tons of oil equivalent, while the proportion of solar and wind energy consumption in the primary energy consumption in Europe is the highest, reaching 8.4 % (172.2 million tons of oil equivalent). Among many

*Corresponding author: jianlunxu@163.com

Tr Ren Energy, 2022, Vol.8, No.2, 84-95. doi: 10.17737/tre.2022.8.2.00140

countries in the world, China's solar and wind energy consumption is 143.5 million tons of oil equivalent, ranking first in the world. The proportion of solar and wind energy consumption in primary energy consumption in Germany is the highest, which is 14.6 % (47.3 million tons of oil equivalent).

Solar energy and wind energy can be used to generate electricity as alternative energy as an alternative to coal. As the power device of many large and small machinery, internal combustion engines are mainly fueled by oil, and new alternative fuels for vehicles need to be found [2]. At present, vehicle alternative fuels can be divided into three categories, *i.e.,* gas (like natural gas, hydrogen) [3,4], battery (such as pure electric and fuel cells) [5,6], and alcohols (methanol, ethanol, butanol, dimethyl ether) [7,8]. Methane and alcohol alternative fuels are essentially hydrocarbon fuels. Compared with gasoline and diesel, they will reduce CO, $CO_2$ and unburned hydrocarbons (HC) emissions during combustion. When emission regulations are more stringent, these alternative fuels are no longer applicable. Hydrogen only contains hydrogen, and the product after combustion is water, which is a real clean energy.

Hydrogen as fuel has the advantages of high efficiency, no pollution, high calorific value and easy access. Hydrogen is an ideal alternative fuel for vehicles, but due to its low density, in order to improve its energy density per unit volume, it is necessary to use high-pressure storage technology. High pressure means high risk. From hydrogen production to storage and transportation to use, every step should consider the safety of hydrogen. Generally speaking, hydrogen security includes hydrogen supply station security, hydrogen supply system (equipment for storing and transporting hydrogen, combination of pipelines and accessories) security, hydrogen transportation system security, collision security and vehicle security. The hydrogen safety in this paper mainly refers to the hydrogen safety of hydrogen fuel cell vehicles. The safety problems of fuel cell vehicles mainly include four aspects: hydrogen storage safety, hydrogen transportation safety, hydrogen collision safety and hydrogen application. In order to make the evaluation of hydrogen safety more comprehensive and intuitive, this study established a hydrogen safety evaluation model.

## Construction of Hydrogen Safety Evaluation Model

The main construction idea of hydrogen safety evaluation model is as follows. Firstly, hydrogen safety is divided into five safety levels according to the gradient theory, and then the appropriate primary and secondary evaluation indexes are selected according to the linear correlation degree. Then, the weight of each evaluation index is calculated by analytic hierarchy process (AHP). Finally, the membership matrix of power following energy management strategy is determined according to the official statistics, simulation data and entity store survey data under power following strategy, and the hydrogen safety level of power following strategy is obtained.

### Hydrogen Safety Grade

Hydrogen safety means that there is no danger, harm or loss in the process of using hydrogen. There are no hidden dangers in storage and use, which are exempt from unacceptable hazards. Hydrogen safety is the control of the damage to human life, material and the environment that the operating level of the system may cause to an acceptable level. Therefore, hydrogen safety is subjective dynamic fuzzy. If we want to

accurately evaluate hydrogen safety, we must well define the safety levels of storage, use, and collision. Hydrogen safety experts believe that the safety state of hydrogen can be divided into grades according to the cascade theory. Hydrogen safety can usually be divided into five or seven grades. Among them, the five levels mainly include very safe, safe, general, unsafe and very unsafe. The seven grades are divided into seven levels as very safe, safe, safer, general, less safe, unsafe and very unsafe. This paper chooses the first classification system.

## Hydrogen Safety Evaluation Principles

To establish a comprehensive evaluation index system of hydrogen safety, a set of representative indicators that can reflect the impact of various aspects of hydrogen safety (such as storage, transportation, collision and application) is selected first. These indicators can accurately show the quantitative judgment of the evaluation objectives of hydrogen safety [9]. Therefore, the selection of hydrogen safety comprehensive evaluation index should follow the following principles:

(1) Scientific: When selecting hydrogen safety evaluation indexes, the number of typical representative indexes should be appropriate and reasonable. On the other hand, must be able to accurately reflect the evaluation objectives, scientific basis for support.

(2) Distinguishing independence: Each factor and sub-factor should not only have its own independence, but also have a certain correlation with other factors and sub-factors. There are levels and depths between evaluation factors and sub-factors, forming a complete and independent system.

(3) Comparative quantitative practice: The indicators can be compared with each other. Qualitative analysis and quantitative analysis can be conducted. In addition, the selected indicators must be simple and easy to take, practical operability, for us to carry out statistics and analysis.

(4) Practical and effective: The purpose of hydrogen safety evaluation is to better serve the safety of energy management strategy of extended range fuel cell car, and ultimately achieve the purpose of optimizing energy management strategy. Therefore, we should choose those indicators that can actually help us effectively improve the hydrogen safety of automobiles.

(5) Objective and reliable: In order to make the final evaluation results accurate and effective, and truly have reference value, all selected indicators must ensure the reliability of data sources and the objectivity of evaluation indicators.

The design and determination of evaluation indicators should follow the above principles. The common methods of screening indicators are: qualitative analysis, sorting, correlation analysis and so on. Qualitative analysis method is based on the selected indicators of evaluation principles for qualitative analysis, and deletes some indicators with poor practicability and scientific objectivity [10]. The ranking method ranks all indicators according to importance, practicality and quantifiable degree, and the former is the optional indicator. Correlation analysis needs to classify the indicators, analyze the correlation of the same type of indicators, merge the indicators with high correlation, and finally obtain a relatively reasonable and comprehensive evaluation index system [11].

## Hydrogen Safety Evaluation Method

There are many factors in the hydrogen safety evaluation system of extended-range hydrogen fuel cell vehicles. How to select the indicators is a multi-objective and multi-criteria problem. Therefore, the conventional linear structure was unable to clearly

express the internal relationship of each index and the various evaluation objectives and needs of each evaluation object [12]. In this paper, the extended range fuel cell vehicle hydrogen safety evaluation is prepared to apply AHP three-level hierarchical analysis. The evaluation object is divided into several objectives according to the logical relationship classification, and then each objective is divided into several sub-objectives in turn, forming a complete tree structure of the target layer, the criterion layer and the index layer, until the object can be quantitatively and qualitatively analyzed. There are many methods for hydrogen safety evaluation, such as BP neural network method, multi-objective comprehensive evaluation method, analytic hierarchy process, fuzzy comprehensive evaluation method, and expert evaluation method. Each method has its own advantages and disadvantages [13]. According to the characteristics of hydrogen security, the analytic hierarchy process is finally selected.

Analytic Hierarchy Process (AHP) can deal with complex and fuzzy problems simply and effectively, which is suitable for the problems that cannot be quantitatively analyzed. This is a simple, effective and practical multi-criteria decision-making method proposed by Professor T. L. Saaty [14]. Usually there are many factors in a system, and the evaluation of the system is composed of the weight ratio of each target. The objective evaluation results of the system are composed of the evaluation results of each sub-objective according to the weight ratio, so a complete multi-level tree evaluation model is obtained. The establishment of multi-level tree evaluation model often uses analytic hierarchy process (AHP). Analytic hierarchy process has the following characteristics [15]:

(1) Not complex and understandable. AHP analytic hierarchy process is simple, and four steps are clear. The analysis process is clear and easy to understand. Moreover, the analytic hierarchy process software can help us establish the model, which uses the root method or sum product method for weight calculation, making the calculation results more scientific and effective.

(2) Flexible and practical. AHP analytic hierarchy process can not only quantitatively analyze but also qualitatively analyze. It can use the relative scale to consider the non-quantifiable factors and theoretical factors. All the factors are organically combined. It breaks the traditional thinking mode and proves that it can be used not only for quantitative analysis but also for qualitative analysis. It is widely used in material distribution, overall analysis, program evaluation and planning scenarios.

(3) Systematic. There are three types of decision-making: The first is to treat the problem as a whole system, so as to make decisions in the research environment of the target system, including all components of the system and the relationship between them. The second is the causal inference. In most of the less complex decisions, the causal logic is basic, simple and convenient, making it the basis of thinking for people to judge and choose things in daily life. The last one is the way of decision-making thinking, because most of the systems have hierarchical relationships. AHP can reflect the decision-making characteristics of such systems, and can be extended and studied more complex systems.

The analytic hierarchy process is modeled according to the following four steps:

(1) The first step is to establish a hierarchical structure model;

(2) The second step constructs all the judgment matrix of each level;

(3) The third step is to conduct hierarchical single sorting and consistency test according to the judgment matrix;

(4) The fourth step is hierarchical sorting and consistency test.

## Hydrogen Safety Index

In general, hydrogen safety evaluation includes four aspects: hydrogen storage, hydrogen transportation, hydrogen collision safety and hydrogen application. According to these four first-level hydrogen safety evaluation indexes, the following four first-level hydrogen safety evaluation indexes and eight second-level evaluation indexes are set up.

*Hydrogen Storage*

Hydrogen storage is divided into hydrogen storage in hydrogenation station and vehicle storage. At present, there are three main hydrogen storage methods, including high pressure hydrogen storage method, liquid hydrogen storage method and solid hydrogen storage method. High-pressure hydrogen storage method, also known as gaseous hydrogen storage method, is to store hydrogen in a specific container with high pressure, similar to CNG cylinders of natural gas vehicles. Its advantage is that compared with the other two storage methods, it has low cost and high hydrogen storage density, and its disadvantage is relatively low security. The second method of liquid hydrogen storage is to liquefy hydrogen at the ultra-low temperature of 20.28 K (− 252.77 ℃), and then it is stored in a specific cryogenic vessel. Its hydrogen storage density is the largest of the three methods, but it is high cost and has a large subsidiary system, so it is not suitable for vehicles. The third solid hydrogen storage method, according to the physical adsorption or chemical reaction mechanism of solid hydrogen, hydrogen is stored in some specific solid materials, and then released through the corresponding reaction when used. Solid-state storage is often safe, efficient and high-density, which is the most promising storage method after gaseous storage and liquid storage. At present, the common solid hydrogen storage materials include alloys, nanoparticles and other materials. Its advantages are relatively safe and have good stability, and the disadvantage is high cost [16].

*Hydrogen Transportation*

There are many commonly used hydrogen production methods. The most commonly used methods are steam reforming of natural gas and electrolysis of water. Large quantities of hydrogen production need to transport hydrogen from the hydrogen station to the hydrogenation station. The most common way of hydrogen transportation is through the pipeline, that is, from the hydrogen storage equipment through the pipeline, gas valve, pressure relief valve and other devices to the fuel cell hydrogen supply. The material and pressure of hydrogen transmission pipeline are the two most critical factors in the process of hydrogen transmission. Due to the small volume energy density of hydrogen itself and the need for high pressure transportation, it is easy to produce "hydrogen embrittlement" phenomenon on the pipe in this process [17].

*Hydrogen Collision*

Hydrogen is likely to collide whether in the process of transportation or in the process of vehicle use. Hydrogen storage or transmission device is easily damaged to produce hydrogen leakage.

(1) Leakability: Hydrogen is the lightest gas, which is more prone to small pore leakage than other fuel gases. Once leakage occurs, hydrogen will rapidly diffuse.

(2) High voltage: For extended-range hydrogen fuel cell vehicles, the vehicle is equipped with a high voltage power circuit, and the voltage of the energy storage system

composed of power batteries is far beyond the safety voltage. Therefore, accidents such as electric shock, short circuit and electrolyte leakage may occur.

(3) Personnel protection: The different structure of extended-range hydrogen fuel cell vehicle has an impact on the activity space and body characteristics of personnel in the vehicle.

(4) Hydrogen storage vessel protection: High-pressure hydrogen storage vessels should use sufficient strength of fixed brackets and seatbelts. When subjected to impact, high-pressure hydrogen storage vessels will not have a large displacement, resulting in fracture deformation of the transmission line and a large amount of hydrogen leakage.

*Hydrogen Applications*

Hydrogen application safety refers to the safety of hydrogen when the vehicle is running. The use of hydrogen fuel in the clearing of vehicles and other transport vehicles will increase hydrogen in the atmosphere, leading to an expansion of the ozone hole. However, the continuous development of new fuel cell technologies and land absorption are considered to eliminate this effect. This article mainly refers to the safety in the automobile application process.

## Calculation of Index Importance and Determination of Weight in Hydrogen Safety Model

According to the selection of four first-level rating indicators and eight second-level rating indicators, the comprehensive evaluation structure of hydrogen security is shown in the figure 1:

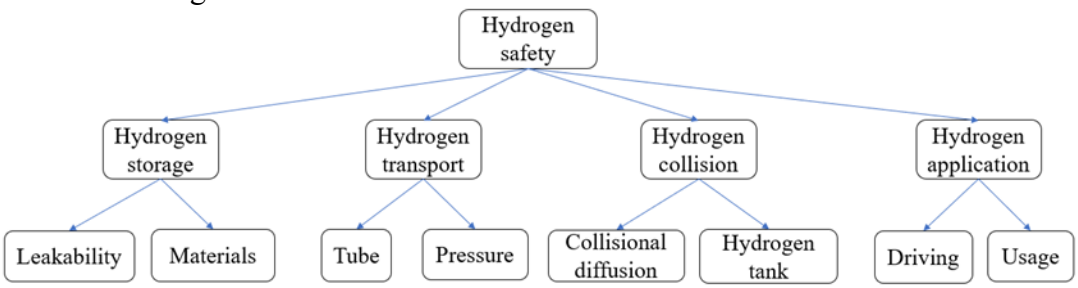


**Figure 1.** Comprehensive evaluation system diagram of hydrogen safety

The determination of weight has a direct impact on the final research results. Hydrogen safety is the target level A, and the four influencing factors of hydrogen storage, hydrogen transportation, hydrogen collision and hydrogen application are selected as the quasi-target level B, while its sub-factor leakage, hydrogen storage material, pipe material, pressure, collision diffusion, hydrogen tank protection, driving and use are selected as the sub-factor level C. The first step is to determine the weight of B to A, and then determine the weight of C to B. Finally, the weight of C to A is comprehensively determined to obtain the final weight of each sub-factor layer and determine their importance. The calculation of importance can directly use the software AHP to input the target layer, and the single-level sorting is used to judge the matrix consistency, and the calculation results are directly obtained and then the results are exported. The importance calculation can also normalize the matrix without software, and the weight of the index can be obtained after normalization. Each column is normalized.

In this paper, the sum product method is used to calculate, and the AHP results are used to make the index weight (Table 1).

**Table 1.** First level index weight table

| Hydrogen safety | Hydrogen storage | Hydrogen transport | Hydrogen collision | Hydrogen application |
|---|---|---|---|---|
| Hydrogen storage | 1 | 3 | 5 | 7 |
| Hydrogen transport | 1/3 | 1 | 3 | 7 |
| Hydrogen collision | 1/5 | 1/3 | 1 | 3 |
| Hydrogen application | 1/7 | 1/7 | 1/3 | 1 |
| Single layer weights | 0.507 | 0.296 | 0.144 | 0.053 |

The satisfaction judgment matrix is:

$$A = \begin{bmatrix} 1 & 3 & 5 & 7 \\ 1/3 & 1 & 3 & 5 \\ 1/5 & 1/3 & 1 & 3 \\ 1/7 & 1/5 & 1/3 & 1 \end{bmatrix} \quad B_1 = \begin{bmatrix} 1 & 3 & 5 & 7 \\ 0.333 & 1 & 3 & 5 \\ 0.2 & 0.333 & 1 & 3 \\ 0.143 & 0.2 & 0.333 & 1 \end{bmatrix}$$

Normalized processing

$$k_1 = \begin{bmatrix} 1+3+5+7 \\ 0.333+1+3+5 \\ 0.2+0.333+1+3 \\ 0.143+0.2+0.333+1 \end{bmatrix} = \begin{bmatrix} 16 \\ 9.333 \\ 4.533 \\ 1.676 \end{bmatrix}$$

$$K_1 = \begin{bmatrix} 0.507 \\ 0.296 \\ 0.144 \\ 0.053 \end{bmatrix}$$

The weight vector set of $B_1$ is $K_1$ = (0.507, 0.296, 0.144, 0.053). The above is the weight of target layer B to target layer A, and the weight of sub-factor layer C to target layer B can be obtained. Tables 2 - 5 are the weight for secondary indicators.

**Table 2.** Weight of hydrogen storage

| Hydrogen storage | Leakability | Materials |
|---|---|---|
| Leakability | 1 | 3 |
| Materials | 1/3 | 1 |
| Single layer weights | 0.75 | 0.25 |

**Table 3.** Weight of hydrogen transportation

| Hydrogen transport | Tube | Pressure |
|---|---|---|
| Tube | 1 | 4 |
| Pressure | 1/4 | 1 |
| Single layer weights | 0.8 | 0.2 |

**Table 4.** Weight of Hydrogen collision

| Hydrogen collision | Collisional diffusion | Hydrogen tank |
|---|---|---|
| Collisional diffusion | 1 | 2 |
| Hydrogen tank | 1/2 | 1 |
| Single layer weights | 0.667 | 0.333 |

**Table 5.** Weight of hydrogen application

| Hydrogen application | Driving | Usage |
|---|---|---|
| Driving | 1 | 2 |
| Usage | 1/2 | 1 |
| Single layer weights | 0.667 | 0333 |

The weight solving process of sub-factor layer C to target layer B is similar to that of target layer B to target layer A. In order to highlight the research focus, each weight vector set is given directly.

The weight vector set of hydrogen storage is: $K_2 = (0.75, 0.25)$;

The weight vector set of hydrogen transportation is: $K_3 = (0.8, 0.2)$;

The weight vector set of hydrogen collision is: $K_4 = (0.667, 0.333)$;

The weight vector set of hydrogen application is: $K_5 = (0.667, 0.333)$;

According to the weight of sub-factor layer C to target layer B and the weight of target layer B to target layer A, the weight of each sub-factor set C to target layer A can be determined. The results are shown in Table 6:

**Table 6.** Weight summary table

| Target layer A | Quasi-target layer B | The weight of B in A | Sub-factor C | The weight of C in B | The weight of C in A |
|---|---|---|---|---|---|
| Hydrogen safety evaluation index | Hydrogen storage | 0.507 | Leakability | 0.75 | 0.3803 |
| | | | Materials | 0.25 | 0.1267 |
| | Hydrogen transport | 0.296 | Tube | 0.8 | 0.2368 |
| | | | Pressure | 0.2 | 0.0592 |
| | Hydrogen collision | 0.144 | Collisional diffusion | 0.667 | 0.0960 |
| | | | Hydrogen tank | 0.333 | 0.0480 |
| | Hydrogen application | 0.053 | Driving | 0.667 | 0.0354 |
| | | | Usage | 0.333 | 0.0176 |

## Hydrogen Safety Level under Power Following Strategy

This paper obtains the statistical results (Table 7) by consulting literature and online data, investigating the physical stores in Zhengzhou City, Henan Province, China, and simulating the model under the power following strategy.

**Table 7.** The number of vehicles in each index under the power tracking strategy

| | Evaluation set | | | | |
|---|---|---|---|---|---|
| | Very unsafe | Unsafe | General | Safe | Very safe |
| Hydrogen storage | 23 | 37 | 46 | 74 | 40 |
| Hydrogen transport | 32 | 23 | 44 | 75 | 26 |
| Hydrogen collision | 24 | 64 | 46 | 53 | 13 |
| Hydrogen application | 11 | 39 | 68 | 23 | 59 |
| Leakability | 30 | 44 | 52 | 39 | 35 |
| Materials | 33 | 55 | 52 | 37 | 23 |
| Tube | 37 | 11 | 75 | 29 | 48 |
| Pressure | 36 | 15 | 45 | 65 | 39 |
| Collisional diffusion | 45 | 62 | 48 | 33 | 12 |
| Hydrogen tank | 25 | 48 | 35 | 69 | 23 |
| Driving | 26 | 60 | 58 | 42 | 14 |
| Usage | 23 | 36 | 69 | 47 | 25 |

The membership degree can be obtained by applying fuzzy mathematics method through quantitative indicators, as shown in Table 8:

**Table 8.** The satisfaction evaluation set of each level index

| | Evaluation set | | | | |
|---|---|---|---|---|---|
| | Very unsafe | Unsafe | General | Safe | Very safe |
| Hydrogen storage | 0.115 | 0.135 | 0.18 | 0.37 | 0.2 |
| Hydrogen transport | 0.16 | 0.115 | 0.22 | 0.375 | 0.13 |
| Hydrogen collision | 0.12 | 0.32 | 0.23 | 0.265 | 0.065 |
| Hydrogen application | 0.055 | 0.195 | 0.34 | 0.115 | 0.295 |
| Leakability | 0.15 | 0.22 | 0.26 | 0.195 | 0.175 |
| Materials | 0.165 | 0.275 | 0.26 | 0.185 | 0.115 |
| Tube | 0.185 | 0.055 | 0.375 | 0.145 | 0.24 |
| Pressure | 0.18 | 0.075 | 0.225 | 0.325 | 0.195 |
| Collisional diffusion | 0.225 | 0.31 | 0.24 | 0.165 | 0.06 |
| Hydrogen tank | 0.125 | 0.24 | 0.175 | 0.345 | 0.115 |
| Driving | 0.13 | 0.3 | 0.29 | 0.21 | 0.07 |
| Usage | 0.115 | 0.18 | 0.345 | 0.235 | 0.125 |

According to Table 8, the single factor evaluation matrix $R_1$ of hydrogen safety evaluation index can be obtained:

$$R_1 = \begin{bmatrix} 0.115 & 0.135 & 0.18 & 0.37 & 0.2 \\ 0.16 & 0.115 & 0.22 & 0.375 & 0.13 \\ 0.12 & 0.32 & 0.23 & 0.265 & 0.065 \\ 0.055 & 0.195 & 0.34 & 0.115 & 0.295 \end{bmatrix}$$

Similarly, the single factor evaluation matrix of hydrogen storage ($R_2$), hydrogen transportation ($R_3$), hydrogen collision ($R_4$) and hydrogen application ($R_5$) safety indicators can be obtained:

$$R_2 = \begin{bmatrix} 0.15 & 0.22 & 0.26 & 0.195 & 0.175 \\ 0.165 & 0.275 & 0.26 & 0.185 & 0.115 \end{bmatrix}$$

$$R_3 = \begin{bmatrix} 0.185 & 0.055 & 0.375 & 0.145 & 0.24 \\ 0.18 & 0.075 & 0.225 & 0.325 & 0.195 \end{bmatrix}$$

$$R_4 = \begin{bmatrix} 0.225 & 0.31 & 0.24 & 0.165 & 0.06 \\ 0.125 & 0.24 & 0.175 & 0.345 & 0.115 \end{bmatrix}$$

$$R_5 = \begin{bmatrix} 0.13 & 0.3 & 0.29 & 0.21 & 0.07 \\ 0.115 & 0.18 & 0.345 & 0.235 & 0.125 \end{bmatrix}$$

The hydrogen safety level 1 evaluation is as follows:

$$K_1 R_1 = (0.507,\ 0.296,\ 0.144,\ 0.053) \begin{bmatrix} 0.115 & 0.135 & 0.18 & 0.37 & 0.2 \\ 0.16 & 0.115 & 0.22 & 0.375 & 0.13 \\ 0.12 & 0.32 & 0.23 & 0.265 & 0.065 \\ 0.055 & 0.195 & 0.34 & 0.115 & 0.295 \end{bmatrix}$$

$$= (0.1259, 0.1589, 0.2075, 0.428, 0.1649)$$

Hydrogen storage:

$$K_2 R_2 = (0.75, 0.25) \begin{bmatrix} 0.15 & 0.22 & 0.26 & 0.195 & 0.175 \\ 0.165 & 0.275 & 0.26 & 0.185 & 0.115 \end{bmatrix}$$

$$= (0.154,\ 0.234,\ 0.26,\ 0.193,\ 0.16)$$

Hydrogen transport:

$$K_3 R_3 = (0.8, 0.2) \begin{bmatrix} 0.185 & 0.055 & 0.375 & 0.145 & 0.24 \\ 0.18 & 0.075 & 0.225 & 0.325 & 0.195 \end{bmatrix}$$

$$= (0.184,\ 0.059,\ 0.181,\ 0.345,\ 0.231)$$

Hydrogen collision:

$$K_4R_4 = (0.667,0.333)\begin{bmatrix}0.225 & 0.31 & 0.24 & 0.165 & 0.06\\ 0.125 & 0.24 & 0.175 & 0.345 & 0.115\end{bmatrix}$$
$$= (0.192,\ 0.287,\ 0.218,\ 0.225,\ 0.078)$$

Hydrogen application:

$$K_5R_5 = (0.667,0.333)\begin{bmatrix}0.13 & 0.3 & 0.29 & 0.21 & 0.07\\ 0.15 & 0.18 & 0.345 & 0.235 & 0.125\end{bmatrix}$$
$$= (0.125,\ 0.26,\ 0.308,\ 0.218,\ 0.085)$$

According to the principle of maximum membership degree and the first-level fuzzy evaluation, under the power following strategy, the membership degree of hydrogen storage index corresponding to "general" is the highest with a value of 0.26. The membership degree of hydrogen transport index corresponding to "safety" is the highest, which is 0.345. The membership degree of hydrogen collision safety corresponding to "unsafe" is the highest, which is 0.287. The membership degree of hydrogen application corresponding to "general" is the highest with a value 0.308.

According to the secondary fuzzy comprehensive evaluation matrix:

$$B = (0.507,\ 0.296,\ 0.144,\ 0.053)\begin{bmatrix}0.154 & 0.234 & 0.260 & 0.193 & 0.160\\ 0.184 & 0.059 & 0.181 & 0.345 & 0.231\\ 0.192 & 0.287 & 0.218 & 0.225 & 0.078\\ 0.125 & 0.260 & 0.308 & 0.218 & 0.085\end{bmatrix}$$
$$= (0.1654,\ 0.1922,\ 0.2353,\ 0.2407,\ 0.168)$$

From the comprehensive evaluation matrix B, it can be seen that the value of "relatively safe" is 0.2407, which is the maximum value, and the value of "general" is 0.2353, which is second only to the maximum value. The evaluation of hydrogen storage index is general, the evaluation of hydrogen transportation index is safe, the evaluation of hydrogen collision safety index is unsafe, and the evaluation of hydrogen application index is general safety. Therefore, the comprehensive evaluation of hydrogen safety under power following strategy is "relatively safe" and tends to "general safety".

## CONCLUSIONS

(1) According to the linear correlation, four first-level evaluation indexes and eight second-level evaluation indexes affecting the hydrogen safety level are determined to establish the structural system.

(2) The selected evaluation indexes are stratified by objectives, and the judgment matrix is constructed. The root method is used to obtain the feature vector of the judgment matrix. The consistency test is used to calculate the weight of the second level. Finally, the hydrogen safety evaluation model is constructed.

(3) The hydrogen safety evaluation model is constructed by using the analytic hierarchy process, and the software simulation and the investigation results of the physical store are analyzed. Finally, the hydrogen safety level under the power following strategy is determined to be relatively safe and biased towards general safety.

## Acknowledgements

This research was supported by Special support plan for high-level talents of Henan Province-"ZHONGYUAN Thousand Talent Program (ZYQR201810075), and "ZHONGYUAN Talent Program" (ZYYCYU202012112).

## CONFLICTS OF INTEREST

The authors declare that there is no conflict of interests regarding the publication of this paper.

## REFERENCES

[1] BP p.l.c. (2019). *BP Statistical Review of World Energy 2019: an unsustainable path* https://www.bp.com/en/global/corporate/news-and-insights/press-releases/bp-statistical-review-of-world-energy-2019.html (accessed on 3/22/2022)

[2] Peng, L., Liu, F., Zhou, M., Li, M., Zhang, Q., and Denise, L. (2021). Alternative-energy-vehicles deployment delivers climate, air quality, and health co-benefits when coupled with decarbonizing power generation in China. *One Earth*, 4(08), 1127-1140. DOI: https://doi.org/10.1016/j.oneear.2021.07.007

[3] Chen, Z., Zhang, T., Wang, X., Chen, H., Geng, L., and Zhang, T. (2021). A comparative study of combustion performance and emissions of dual-fuel engines fueled with natural gas/methanol and natural gas/gasoline. *Energy*, 237, 121586. DOI: https://doi.org/10.1016/j.energy.2021.121586

[4] Karthikeyan, S., and Periyasamy, M. (2021). Impact on the power and performance of an internal combustion engine using hydrogen. *Materials Today: Proceedings*. DOI: https://doi.org/10.1016/j.matpr.2021.02.356

[5] Gürsel, Ş., and Mert, A.Ö. (2022). Experimental and numerical study of energy and thermal management system for a hydrogen fuel cell-battery hybrid electric vehicle. *Energy*, 28(B), 121794. DOI: https://doi.org/10.1016/j.energy.2021.121794

[6] Tang, Q., Yang, Y., Luo, C., Yang, Z., and Fu, C. (2022). A novel electro-hydraulic compound braking system coordinated control strategy for a four-wheel-drive pure electric vehicle driven by dual motors. *Energy*, 241, 122750. DOI: https://doi.org/10.1016/j.energy.2021.122750

[7] Nuthan Prasad, B. S., Pandey, J. K., and Kumar, G. N. (2020). Impact of changing compression ratio on engine characteristics of an SI engine fueled with equi-volume blend of methanol and gasoline. *Energy*, 191, 116605. DOI: https://doi.org/10.1016/j.energy.2019.116605

[8] Verma, A., Dugala, N. S., and Singh, S. (2022). Experimental investigations on the performance of SI engine with Ethanol-Premium gasoline blends. *Materials Today: Proceedings*, 48, 1224-1231. DOI: https://doi.org/10.1016/j.matpr.2021.08.255

[9] Qin, G., Zhang, M., Yan, Q., Xu, C., and Daniel, M.K. (2021). Comprehensive evaluation of regional energy internet using a fuzzy analytic hierarchy process based on cloud model: A case in China. *Energy*, 228, 120569. DOI: https://doi.org/10.1016/j.energy.2021.120569

[10] Nachiappan, S. and Ramakrishnan, R. (2012). A review of applications of Analytic Hierarchy Process in operations management. *International Journal of Production Economics*, 138(2): 215-241. DOI: https://doi.org/10.1016/j.ijpe.2012.03.036
[11] Zhang, C., Sung-Kwun, O., and Fu, Z. (2021). Hierarchical polynomial-based fuzzy neural networks driven with the aid of hybrid network architecture and ranking-based neuron selection strategies. *Applied Soft Computing*, 113(B), 107865. DOI: https://doi.org/10.1016/j.asoc.2021.107865
[12] Gan, Y., Meng, B., Chen, Y., and Sun, F. (2022). An intelligent measurement method of the resonant frequency of ultrasonic scalpel transducers based on PSO-BP neural network. *Measurement*, 190, 110680. DOI: https://doi.org/10.1016/j.measurement.2021.110680
[13] Zheng, Y., and Wang, D. (2022). A survey of recommender systems with multi-objective optimization. *Neurocomputing*, 474, 141-153.
[14] Grošelj, P. (2021). Symmetric projection group approach for promoting homogeneity in the analytic hierarchy process. *Computers & Operations Research*, 133, 105343. DOI: https://doi.org/10.1016/j.cor.2021.105343
[15] Havle, C.A. and Kılıç, B. (2019). A hybrid approach based on the fuzzy AHP and HFACS framework for identifying and analyzing gross navigation errors during transatlantic flights. *Journal of Air Transport Management*, 76, 21-30. DOI: https://doi.org/10.1016/j.jairtraman.2019.02.005.
[16] Hassan, I.A., Haitham, S.R, Mohamed, A.S., and Daniel, H. (2021). Hydrogen storage technologies for stationary and mobile applications: Review, analysis and perspectives. *Renewable and Sustainable Energy Reviews*, 149, 111311. DOI: https://doi.org/10.1016/j.rser.2021.111311.
[17] Jeffrey, V., Lim, F., Liu, L., Sonia, J., Zhou, Q., Ruth, K., Zhang, M., Li, H., Dong, F., Matthew, S.D., and Andrej, A. (2020). Hydrogen embrittlement of an automotive 1700 MPa martensitic advanced high-strength steel. *Corrosion Science*, 171, 108726. DOI: https://doi.org/10.1016/j.corsci.2020.108726.



Trends in Renewable Energy
OPEN ACCESS ISSN: 2376-2144
Peer-Reviewed Review Article futureenergysp.com/index.php/tre

# A Review of Engine Emissions Testing Methods for Environmental Sustainability

Minghao Wang*

*School of Mechanical Engineering/Institute of Vehicles and New Energy Technology, North China University of Water Resources and Electric Power, Zhengzhou City, Henan, China*

Received February 25, 2022; Accepted March 23, 2022; Published March 28, 2022

With the increase of vehicle ownership, vehicle emission pollution has become a major source of air pollution. The control of automobile pollutant emissions is one of the effective methods to reduce air pollution. Domestic and foreign exhaust pollutant testing methods for in-use vehicles have been gradually developed from the original idling method to the double-idling method and the simple working condition method. There are many methods to test the exhaust pollutants of in-use vehicles, but the test operation cycle, gas analysis principle, cost, application occasions and the accuracy level of various testing methods are different. This paper introduces the idling method, the working condition method and the on-board emission testing method for detecting vehicle emission pollutants. Two optimized methods for detecting automotive emission pollutants (namely the double-idle method and the simple transient working condition method) are also introduced.

*Keywords: Emission characteristics; Detection methods; Air pollution; Idling method; Working condition method; On-board emission testing method*

## Introduction

In recent years, with the continuous development of the automobile industry and the increase of the average gross national product (GNP), the number of vehicles is also growing. In 2015, the number of motor vehicles in China was 273 million, of which 172 million were cars, accounting for 61.65%. By 2020, the number of motor vehicles in China reached 372 million, and the number of cars in China reached 281 million in 2020, accounting for 75.54%. In the past five years, China's car ownership has increased by 63.4% year-on-year. There are 70 cities in China with more than 1 million cars. There are 31 cities with more than 2 million vehicles and 13 cities with more than 3 million vehicles, including more than 5 million vehicles in Beijing, Chengdu and Chongqing, and more than 4 million vehicles in Suzhou, Shanghai and Zhengzhou. All these data can clearly show that China's car ownership has been showing a very rapid growth trend. In the process of the rapid growth of car ownership, the emission and concentration of automobile pollutants are also gradually increasing, which will cause serious pollution to urban air quality. So, the problem of urban air pollution caused by car emissions has become very serious [1].

Gasoline engine emissions mainly include hydrocarbons, carbon monoxide and nitrogen oxides. In order to solve the problem of automobile emission pollution, scholars in various countries have shifted their research focus to alternative fuels. At present, the

*Corresponding author: wang22310@ 163.com

Tr Ren Energy, 2022, Vol.8, No.2, 96-106. doi: 10.17737/tre.2022.8.2.00141

main alternative fuels include methanol, ethanol, hydrogen, natural gas and dimethyl ether. It was found that the mass fraction of C atom in methanol and ethanol branches was small, which could reduce CO and soot emissions. Moreover, the high oxygen content in methanol and ethanol is more conducive to promoting the complete combustion of fuel, saving fuel, and greatly improving the exhaust emission performance, with the average reduction of CO and CH compounds by more than 30% **Error! Reference source not found.**, [3]. The high vaporization latent heat of methanol can reduce the combustion temperature, reduce the formation of $NO_x$ compounds, and improve the methanol ratio to obtain better combustion and reduce the formation of HC, CO and soot [4]. However, with the increase of methanol blending ratio, $NO_X$ emission also increases significantly [5]. Compared with gasoline, CO, HC and $NO_x$ emissions of ethanol-blended gasoline fuel are significantly reduced **Error! Reference source not found.**. However, with the increase of ethanol mixing ratio, NOx emission decreases, and CO and HC emissions increase [7]. This makes the engine emission test technology extremely important. A good test method can improve the accuracy of test results and provide a theoretical basis for the control of vehicle emissions.

China is the world's second largest economy. China's economic development has made great achievements in the past decade. At the same time, severe haze occurs frequently in the country, especially in areas with high economic growth. According to monitoring data from China's Ministry of Ecology and Environment, the number of haze days in 74 pilot cities with new air standards accounts for 25% to 50% of the year and is on the rise. Motor vehicle emission standard I was uniformly implemented nationwide in 2000, and motor gasoline standard I and diesel standard I were implemented in 2001 and 2003, respectively. Emission standards have been continuously improved since then. In 2019, the gasoline standard VI and diesel standard VI were implemented [8]. And good exhaust gas testing emission methods can reduce the error of engine emission test values and improve the rate of engine development and improvement.

Different emission testing methods have different emission limits. In order to truly and accurately screen and identify urban high-emission and high-polluting vehicles, the correlation between the emission limits of each testing method should continue to be studied to achieve effective control of motor vehicle emissions.

## Emission Testing Methods

The exhaust of an engine contains harmful gases, liquid particles and solid particulate components. The measurement of harmful gas components such as $CO_2$, HC, $NO_X$, SO, etc. in the exhaust gas is usually analyzed in engine testing as exhaust gas analysis, while the measurement of visible pollutants contained in the exhaust gas is called smoke measurement or exhaust visible pollutant measurement.

### Contaminant Detection Methods

The test methods for the emission of pollutants from automobiles are divided into two types of test methods, *i.e.,* the idling method and the working condition method.

*Idle Speed Detection Method*

The idling method is a method of measuring exhaust pollutants from a vehicle at idling conditions, generally measuring only CO and HC, and using a portable emission

analyzer as the measuring instrument. This method has the advantages of simplicity, cheap and portable measuring device, and short testing time. However, the disadvantage of the idling method is the lack of comprehensive representation of the measurement results. Idle speed method can be used as the environmental protection department of the in-use vehicle emissions testing, as well as a comprehensive automotive repair shop on the vehicle emissions performance and whether the engine is working properly for a simple evaluation method, can not be used as the engine factory emissions measurement standards. It cannot be used as an emission measurement standard for the engine [9].

*Working Condition Test Method*

The working condition method combines a number of common working conditions of a vehicle and the more polluting working conditions for pollutant emission measurement, with a view to evaluating the vehicle emission level comprehensively. At present, there are three major systems of emission regulations in the world, namely, the United States, Japan and the European system. Other countries basically develop their own emission regulations on the basis of the United States and European regulations.

Compared with the idling method, the working condition method can reflect the level of vehicle emissions more comprehensively, which is generally used for the certification of new vehicles and factory sample testing. But the price of its test equipment is often 100-200 times more than the portable emissions analyzer for the idling method. The main equipment used for vehicle emission pollutant testing by the working condition method includes an exhaust sampling system, chassis dynamometer, gas flow analyzer, automatic detection control system, and five gas analyzers. The actual test is carried out by first pre-testing the vehicle to verify the basic conditions of the vehicle and ensure that the vehicle is suitable for emission pollutant testing by the working condition method.

*Vehicle-borne Emission Testing Methods*

Vehicle exhaust testing using a Portable Emissions Measurement System (PEMS) is called Vehicle Emissions Testing. It is directly installed on the car driving on the road, effectively collects various parameters and pollutant emission conditions during the driving process of the vehicle, and clearly expresses the pollutant emission status in the driving process of the vehicle. High sensitivity, good vibration resistance and high sensitivity are the direct advantages of this detection method. This detection method is very widely used [10].

The PEMS system can directly measure the exhaust gases of a vehicle, including CO, CO2, HC, $NO_X$, and particulate matter, as well as the vehicle's driving recorder, location information and speed. The analyzer uses the specificity of the infrared wavelength electromagnetic energy of different gases to further detect pollution levels.

## Exhaust Gas Sampling Methods

*Direct Sampling Method*

The direct sampling method is to insert the sampling probe directly into the engine exhaust pipe which uses the sampling pump to take a certain amount of gas sample directly for feeding into the water separator. The water separator is generally composed of a condenser and a drainage device, which is used to condense and dehumidify the exhaust gas sample, and prevent the interference of the moisture in the exhaust gas sample to the exhaust gas analyzer. After the coarse filter and fine filter, the

dust, solid particle contaminants and liquid particle contaminants in the gas are filtered out. The exhaust gas needs to be dried. As shown in Figure 1, to prevent coalescence and adsorption of HC and other components in the sampling tube, the lower concentration specimen pipeline can be separated and the pipeline system can be heated to 140°C for measuring HC content in gasoline engine exhaust, and 180-200°C for diesel.

The direct sampling method is simple and easy to use, which can be flexibly applied to all operating conditions. It is suitable for continuous observation of changes in exhaust composition due to variable operating conditions. As a standard sampling method, the direct sampling method is widely used in bench tests and idle measurements of heavy vehicles.

However, the adsorption phenomenon in the sampling line of the direct sampling method can cause measurement errors. In order to remove water vapor from the sample gas, a condenser and other devices are required in the sampling system, but condensation tends to coagulate substances with high boiling points in the exhaust gas. Since the operating temperature of the condenser is different, the measured HC concentration will vary.

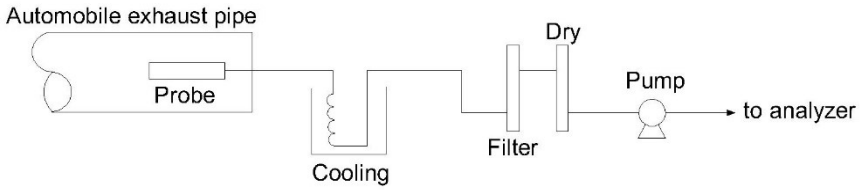


**Figure 1.** Direct sampling exhaust gas analyzer

*Constant Volume Sampling Method*

The constant volume sampling method is also known as variable dilution sampling, and there are three common types of variable dilution sampling devices: constant volume samplers with positive displacement pump (PDP-CVS), constant volume samplers with critical flow venturi (CFV-CVS), and constant volume samplers with controlling stable flow by volume orifice (CFO-CVS). The CFV system is less affected by temperature and is relatively simple. However, changing the total flow requires replacing the Venturi tube, and the total flow of the system can only be changed in stages.

Emission regulations around the world now require sampling with a constant volume sampling (CVS) system. A typical exhaust gas analyzer measures the concentration of the component in the exhaust and then calculates the total emission of the component based on the exhaust flow. This needs to be achieved with the engine in steady state operation. In a non-steady state, the measured concentration curve and the exhaust flow curve can theoretically be integrated over time to calculate the total. However, in actual operation, this can lead to large errors due to the variation of exhaust pressure with operating conditions, differences in the dynamic response lag of the sampling system and the measuring instrument, and the fact that the mixture concentration curve of the sampled gas does not reproduce the temporal characteristics of the engine emissions [11] .

So, the researchers used a method of measuring the average to solve the problem. The most intuitive way to do this is to collect all the exhaust gas from 1 standard test cycle into an air bag. Then, the concentration of each pollutant in the air bag is measured at the end of the test cycle and multiplied by the total amount of diluted exhaust that

flowed through the CVS system to get the total amount of each pollutant in the engine during the measurement.

The constant volume sampling method is a sampling method that approximates the actual state of vehicle exhaust diffusion into the atmosphere. After dilution with air, it is ensured that the density of the diluted gas remains constant at a constant temperature. A fixed volume flow of the sample gas is then sent to atmosphere by the action of a constant volume pump. There is a strict proportionality between the sample gas and the flow rate of the constant volume pump. The constant volume sampling method prevents water vapour condensation due to sufficient dilution to contain the interaction between the emission components. However, if the dilution is too strong, the concentration of pollutants in the diluted sample gas will be too low, causing problems such as insufficient sensitivity of the measurement analyzer.

The constant volume sampling method has two systems of CVS-1 and CVS-3. The CVS-1 uses only one type of sampling bag, while the CVS-3 sampling system uses three sampling bags, allowing for three separate samples for the cold start, stable operation, and hot start phases.

*Full Volume Sampling Methods*

The full volume sampling method involves collecting the entire exhaust from an engine exhaust test into a bag with sufficient volume for analysis [12]. This sampling method allows both the determination of the average concentration of exhaust pollutants and the calculation of emissions. From the time the sample gas is introduced into the bag to the final measurement, it is very likely that HC will be adsorbed in the bag, that reactive components of HC will react or polymerize with each other, and that $NO_x$ will be oxidized. In order to prevent the condensation of water vapor in the sample gas in the bag, the sample gas is cooled with 10-15°C water before entering the bag through a thermal interactor, so the HC with high boiling point is also easily condensed and dissolved in water and then released, causing certain errors.

## Optimized Emission Gas Detection Methods

### Double Idle Method

The exhaust pollutant testing methods for in-use vehicles have been gradually developed from the original idling method to the double-idling method in China and abroad [[13]. It is a method to measure the volume concentration of CO and HC in the exhaust of in-use vehicles under idling conditions and high idling conditions (*i.e.,* 50% of rated speed). It is proposed by the International Organization for Standardization in ISO3929 and generally accepted by all countries. In the emission regulations for in-use gasoline vehicles promulgated by the China State Ministry of Environmental Protection, the double-idling method is used as the basic measurement method, which is equivalent to the standard of the EU Regulation 92/55/EEC. The main pollutants measured by the dual-idle method are CO and HC, and China Standard GB8285-2005 requires the use of a Non-Dispersive Infrared (NDIR) analyzer for measuring pollutants by the dual-idle method. The main advantages of the dual idle measurement are that it has low requirements on test instruments, is easy to use, and has a certain recognition rate for high emission measurements [14].

Both the idling method and the double-idling method have the following problems in actual use: (1) The idling and double-idling methods will achieve good results in testing old, technologically outdated vehicles. However, when testing electronically controlled vehicles (such as vehicles equipped with three-way catalytic converters and oxygen sensors), the recognition rate of high pollution measurements is not high. This is because, when the efficiency of the three-way catalytic converters decreases, the idling conditions with relatively low speed of conversion efficiency may still be high, while the conversion efficiency drops sharply for medium and large loads at relatively high RPM. (2) The idle speed method and double idle speed method are not suitable for testing $NO_X$ emissions. The reason is that at idle speed or high idle speed, $NO_X$ emission is small and difficult to detect. (3) The idle speed method and double idle speed method only test the unrepresentative working condition of the car, which cannot reflect the actual working emission of the car. (4) The idle speed method and double idle speed method leave opportunities for carburetor cars to cheat. The owner can lower the mixture concentration by adjusting the carburetor idle speed screw and throttle screw before the test, deviating from the normal idle concentration mixture design state. After passing the test, in order to ensure the smooth start of the vehicle, the operation can be reversed to the original state. (5) The correlation between the idle speed method or double idle speed method and working condition method is poor, and the identification rate of high emission vehicles is relatively low.

### Simple Transient Service Method (VMAS)

In gasoline vehicle exhaust testing, both the simple transient condition method and the double idling method require the use of gas analyzers to analyze pollutant concentrations. The simple transient condition method uses five gas analyzers (HC, CO, $CO_2$, $O_2$, NO), and the double idling method uses four gas analyzers (HC, CO, $CO_2$, $O_2$). The gas analyzer is an important piece of equipment for gasoline vehicle exhaust testing and has a direct impact on the accuracy of the test results, and its routine calibration/inspection is an effective means to ensure equipment compliance and result accuracy. The daily calibration/check is an effective means to ensure the compliance of the equipment and the accuracy of the results [15].

The simple condition method is divided into simple steady state loading condition method and simple transient condition method. The steady state loading condition method mainly checks the HC, CO, $CO_2$ and NO levels of gasoline vehicles while driving. If the emission concentrations of each pollutant are within the limits specified in the standard, the vehicle's test results can be considered as qualified. The transient condition method not only tests the above gases with the analyzer, but also takes into account $O_2$, and the test is done with the participation of a gas flow meter.

The VMAS sampling system for the simple transient condition method can be divided into two parts: One part extracts a small amount of raw emission gas and sends it to the five gas analyzer. The other part extracts the remaining vehicle exhaust after dilution by ambient air and sends it to the gas flow analyzer. After the gas flow analyzer is tested and converted to a standard state flow rate for the dilution flow rate, the original emission gas volume flow rate is calculated as follows.

$$V_R = V_d \times \eta \tag{2.2.1}$$

where: $V_d$-volumetric flow rate of diluted emission gas; η-dilution ratio, and

$$\eta = \frac{O_a - O_d}{O_a - O_r} \tag{2.2.2}$$

where: $O_a$-oxygen content in the environment; $O_d$-diluted oxygen content; $O_r$-original oxygen content.

The system finally takes the emission gas concentration measured by the five-gas analyzer and the raw emission gas flow rate and runs it through the VMAS microprocessor to obtain the mass emission value of the pollutant per second, *i.e.,*

$$m_n = C_m \times \rho_{rn} \times V_r \tag{2.2.3}$$

where $m_n$-mass of emission, g/s; $C_{rn}$-volumetric concentration of the $n^{th}$ substance (CO, $CO_2$, $O_2$, HC, $NO_x$) in the original exhaust; $\rho_{rn}$-density of the $n^{th}$ substance in the original exhaust; $V_r$-volumetric flow rate of the original exhaust gas.

The system calculates the mass of each vehicle's exhaust pollutant on a second-by-second basis according to the above formula during the test, integrates it to obtain the mass of each emission during the entire test cycle, and divides it by the mileage of the test cycle to obtain the emission of each vehicle's exhaust pollutant (g/km).

The routine calibration/checking of the five gas analyzers can have an impact on the results of the simple transient service method [16]-[18]. For example, the accuracy of the five-gas analyzer, the accuracy of the standard gas and the pressure of the standard gas will have an adverse effect on the results of the simple transient method. Taking the standard gas pressure as an example, the five-gas analyzers used in Guangzhou, China are mainly controlled at 0.02 MPa and 0.1 MPa, which control the gas flow into the gas chamber under the limited pressure in line with the equipment set requirements (general flow requirements for about 20 mL/s). If the incoming air pressure does not match the specified air pressure, the calibration/check result will be inaccurate. If the incoming gas pressure is too low, the device response time is too long and the measured value is low. When the incoming gas pressure is too high, some devices have high measured values and the gas consumption is high.

Both the double-idling method and the simple transient working condition method can be used to screen high-emission vehicles. Under the respective determination conditions, the pollutant emissions per unit driving mile of the exceeded vehicles are much higher than those of the attained vehicles, while the pollutant emissions per unit driving mile of the exceeded vehicles of the VMAS are about 1.5 times of those of the exceeded vehicles of the double-idling method. There are still some vehicles with smaller pollutant emissions per unit mile traveled in the double-idling method, and they are at the emission level of the attainment vehicles, which means that the vehicles screened by the simple transient method are really high-emission vehicles. The screening results are more accurate and reasonable, and the results are more obvious when applied to in-use motor vehicles [19], [20].

### Acceleration Simulation Mode (ASM)

In order to meet the emission control requirements for $NO_x$, a loaded test method is required. The simplest loaded test method is the ASM (Acceleration Simulation Mode) steady-state method, which is a combination of two steady-state conditions, 5025 and 2540, developed by the Southwest Research Institute and Sierra Research Institute in California, USA, in 1988. China's emission standards propose the use of ASM as a simple working condition method for in-use vehicle exhaust testing, which includes ASM5025 and ASM2540 two typical equal-speed loaded operating conditions.

(1) 50% of the output power at the ASM5025 operating test speed of 25 km/h and acceleration of 1.475 m/s$^2$ (the maximum acceleration in the FTP-75 cycle) is used as the loading power. For practical convenience, the standard provides for loading at the base mass of the test vehicle, when the loading power P5025 = base mass of the vehicle/148.
(2) 25% of the output power of the ASM2540 at a working test speed of 40 km/h and an acceleration of 1.475 m/s$^2$ is used as the loading power. In practice, the vehicle is loaded at its base mass and the loading power P2540 = base mass of the vehicle/185.

ASM is a load test, which can measure and discriminate the $NO_x$ emission of vehicles, and is better than the idling method or double-idling method in identifying high-emission vehicles. However, the test conditions of the ASM method are at only two vehicle speeds, which are still different from the emission conditions when the vehicle is actually driving. Even if the emissions under these two working conditions pass, it does not guarantee that the emissions under other working conditions also pass. Moreover, the proportion of acceleration and deceleration conditions with poorer emissions in the actual use of the vehicle is larger, so this method cannot determine the superiority or inferiority of emissions during acceleration and deceleration.

Another shortcoming of the ASM is that the method is based on pollutant emission concentrations rather than emission masses. A vehicle with a small engine displacement emits less mass and a vehicle with a larger displacement emits more mass. But it is possible that the emission concentrations are the same. The ASM is thus unfair to vehicles with different engine displacements.

## Transient Working Condition Method

*IM240 Transient Operating Conditions*

The IM240 test condition uses the two peaks of the first 0 to 333 seconds of the Federal Test Procedure (FTP) curve of the U.S. federal test protocol for new car type certification, which has been shortened to 240 seconds with modifications. The operating principle of the test equipment is the same as that required for the new vehicle test. The sampling device and analytical instrumentation are consistent with the new vehicle test. The sampling system is Constant Volume Sampling (CVS). The analytical instrumentation was a Non-Dispersive Infrared (NDIR) analyzer for CO, a Hydrogen Flame Ion Analyzer (FID) for HC, and a Chemiluminescence Analyzer (CLA) for $NO_x$. The final test results are expressed in g/km.

The IM240 characteristic test results have good correlation with FTP results. The correlation factors for the three pollutants can reach: 91.8% for CO, 94.7% for HC, and 84.3% for $NO_x$. At the same time, the dispersion of the IM240 test results for the three pollutants relative to the FTP results is small, so the misclassification rate of IM240 is low. IM240 is a highly technical test method, with expensive equipment, more complicated maintenance, longer testing time, and higher requirements for the testers.

*IM195 Transient Operating Conditions*

The China State Ministry of Environmental Protection has proposed IM195 transient condition in the new in-use vehicle emission standard, which is exactly the same as the first cycle condition in the first stage of the new model type certification condition specified in China Standard GB18352.1-2001 "Emission Limits and Measurement Methods for Light Duty Vehicles (I)" with a cycle test time of 195s (hence named as IM195). It contains a total of 15 working conditions, such as idle speed, acceleration,

deceleration, steady speed, etc., which comprehensively simulates the driving conditions of the vehicle on the road. The test condition curves are shown in Figure 2.

The profile lines in Figure 2 indicate the gear change. The solid line is the theoretical operating condition line, and the dashed line is the actual operating curve of the tested vehicle. Except for the test cycle, the transient conditions IM195 and IM240 use exactly the same gas analysis principles and exhaust gas sampling system.

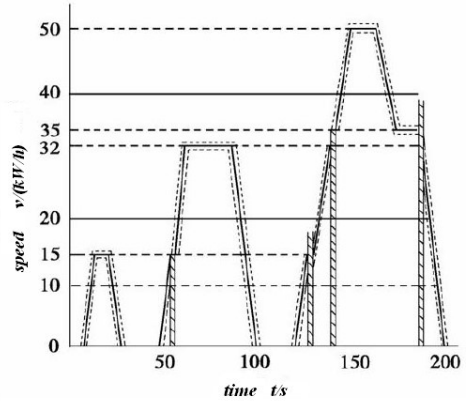


**Figure 2.** Transient working condition method (IM195)

## CONCLUSION

A series of exhaust testing methods for in-use gasoline vehicles are briefly discussed, which includes the no-load idling method, the double-idling method, the loaded method with ASM steady-state operating conditions [21] and VMAS simple transient condition method. Some cities in China (such as Shenyang, Fushun, Anshan, Qingdao, and Shenzhen) have implemented the load test methods for in-use gasoline vehicles, including ASM and IG195 test methods. The advantages and disadvantages of these different test methods can be summarized as follows.

(1) The idling and double-idling methods do not reflect the actual emissions of the vehicle being driven and are not suitable for use in heavily polluted cities.

(2) The investment of ASM method equipment is low, the technology is mature, and the equipment of ASM method can be upgraded to VMAS equipment. So, it is reasonable to apply ASM testing method at this stage.

(3) The investment of VMAS equipment is medium, and the correlation between the test accuracy and the working condition method is good. The accuracy rate is high, and the error rate is only 5% or less (with the accuracy rate of IM240 being 100%). With the increasingly strict emission regulations, this test method will be the inevitable trend in the development of China's in-use vehicle exhaust testing methods.

(4) At present, the exhaust testing method used in China is basically equivalent to the methods used in Europe and the United States. It is the direction of further research to carry out the research on the working conditions of the exhaust testing curve of in-use vehicles, which is suitable for the actual situation of vehicles and the requirements of environmental protection in China.

## CONFLICTS OF INTEREST

The author declares that there is no conflict of interests regarding the publication of this paper.

## REFERENCES


[1] Wu, W. (2021). Analysis of the current situation of China's automobile emission control level and comprehensive countermeasures. *Internal Combustion Engine and Accessories,* 2021(5), 148-149. DOI: 10.19475/j.cnki.issn1674-957x.2021.05.069.

[2] Mohammed, M. K., Balla, H. H., Al-Dulaimi, Z. M. H., Kareem, Z. S., and Al-Zuhairy, M. S. (2021). Effect of ethanol-gasoline blends on SI engine performance and emissions. *Case Studies in Thermal Engineering*, 25, 100891. DOI: 10.1016/j.csite.2021.100891

[3] Yang, Z., Ge, Y., Wang, X., and Liu, J. (2020). Effect of Ethanol Gasoline on Emission Characteristics of China Sixth Direct Injection Gasoline Vehicle. *China Environmental Science,* 40 (12), 5213-5220. DOI:10.19674/j.cnki.issn1000-6923.2020.0575

[4] Zhou, D.Z., Yang, W.M., An, H., Li, J., and Shu, C. (2015). A numerical study on RCCI engine fueled by biodiesel/methanol. *Energy Conversion and Management,* 89, 798-807. DOI: 10.1016/j.enconman.2014.10.054

[5] Iliev, S. (2018). Comparison of Ethanol and Methanol Blending with Gasoline Using Engine Simulation. In (Ed.), *Biofuels - Challenges and oppor*tunities. IntechOpen. DOI: 10.5772/intechopen.81776

[6] Pan, J., Cheng, B., Tao, J., Fan, B., Liu, Y., and Otchere, P. (2021). Experimental Investigation on the Effect of Blending Ethanol on Combustion Characteristic and Idle Performance in a Gasoline Rotary Engine. *Journal of Thermal Science*, 30(4), 1187-1198. DOI: 10.1007/s11630-021-1487-33

[7] Rakopoulos, D. C., Rakopoulos, C. D., Kakaras, E. C., and Giakoumis, E. G. (2008). Effects of ethanol–diesel fuel blends on the performance and exhaust emissions of heavy duty DI diesel engine. *Energy Conversion and Management*, 49(11), 3155-3162. DOI:10.1016/j.enconman.2008.05.023

[8] Zhang, X. and Wang, Q. (2020). Study on the emission reduction effect of vehicle emission control policy in China. *China Population-Resources and Environment,* 30 (5), 98-109.

[9] Zhao, B. and Liu, X. (2017). Analysis of the detection method of automobile emission pollutants. *Automotive maintenance,* 2017(1), 4-8.

[10] Deng, Y. (2018). Detection methods for automotive emission pollutants. *Automotive Practical Technology,* 20, 58-60. DOI:10.16638/j.cnki.1671-7988.2018.20.020

[11] Wang, H.Y., Huang, C., Hu, Q.Y., Li, L., Chen, Y.H., and Xu, J. (2017). Emission correlation between simple transient operating condition method and constant volume full flow dilution sampling (CVS) method for light duty gasoline vehicles. *Environmental Science,* 38 (6), 2294-2300. DOI:10.13227/j.hjkx.201611139

[12] Wu, K.G and Cao, J.M. (2002). *Engine Testing Technology*, People's Traffic Press, Beijing.

[13] Wang, F. (2008). *Research on the testing methods and standards for exhaust pollutants of in-use gasoline vehicles*, Chang'an University, Thesis.

[14] China National Standards. (2005). *Limits and measurement methods for exhaust pollutants from vehicles equipped ignition engine under two-speed idle conditions and simple driving mode condition*. GB 18285-2005
[15] Yu, W.Y., Huang, Q.F., Huang, S.W., and Chen Q.H. (2015). Analysis of daily calibration/checking of five gas analyzers in simple transient working method and its influencing factors. *Analytical Instruments,* 2015(2), 74-79.
[16] Yu, Z., Xu, Z., Sun, L., and Bao, X. (2012). Study on emission degradation pattern of in-use vehicles. *Automotive Engine,* 2012(2), 63-65.
[17] Nong, J. and Shuang, J. (2010). A comparative analysis of double idling method and simple transient working condition method for exhaust gas detection of motor vehicles. *Environmental Engineering* 28(S1), 280-284. DOI:10.13205/j.hjgc.2010.s1.076
[18] Industry Standards - Environmental Protection. (2005). *The principle and method of confirm limits for exhaust pollutants from in-use vehicle equipped ignition engine under simple driving mode conditions*.
[19] Industry Standards - Environmental Protection. (2009). *Emission Limits for Exhaust Pollutants from Light Duty Vehicles with In-use Ignition Engines (Simple Transient Condition Method)*.
[20] Liu, X.H. and Zhu, X.P. (2014). Analysis of in-use motor vehicle exhaust emission detection methods. *Shanxi Electronic Technology,* 2014(4), 59-61.
[21] Wu, X. and Song, J. (2007). Research and development of in-use vehicle exhaust emission testing system with steady-state loading condition method. *Highway Traffic Technology,* 24(6), 131-138.



Trends in Renewable Energy
OPEN ACCESS ISSN: 2376-2144
Peer-Reviewed Article futureenergysp.com/index.php/tre

# Backpropagation Neural Network (BPNN) Algorithm for Predicting Wind Speed Patterns in East Nusa Tenggara

Andri Gunawan,* Suyono Thamrin, Yanif Dwi Kuntjoro, and Abdi Manab Idris

*Department of Energy Security, Faculty Defense Management, Indonesia Defense University, Jakarta 10430, Indonesia*

Received March 8, 2022; Accepted April 4, 2022; Published April 10, 2022

The Paris agreement compels all countries to make major contributions to the zero-emission scheme, a legally binding international treaty on climate change. This fulfilment must be supported by technological developments towards Society 5.0, forcing every country to develop renewable energy (clean energy) on a large scale. One of the renewable energies with the highest efficiency is wind power generation. Its construction requires a large cost, and the best location must consider the high wind speed. East Nusa Tenggara Province is one of the locations in the border area with insufficient electricity. The choice of location was supported by military operations in guarding the border which required a lot of energy. Therefore, it is necessary to predict wind speed patterns based on historical data from the database so that wind power plants can be realized. One of the best methods for long-term prediction of wind speed is the backpropagation neural network (BPPN) method. Wind speed data was used from January 2003 to December 2020 with a total of 216 data sets obtained from NASA. It should be noted that January 2003 to December 2010 data is positioned as input data, while training target data is from January 2011-December 2015. Validation data is determined from January 2016-December 2020. The best predictive architecture model is 8-11-5- 5, learning rate is 0.4 and epoch is 20,000. Prediction accuracy is very good with a mean square error (MSE) value of 0.007634 and a mean absolute percentage error (MAPE) of 11.62783. The highest wind speed was shown in February 2018 as 10.75 m/s.

*Keywords: BPPN; Wind Speed; MSE; MAPE; East Nusa Tenggara*

## Introduction

Adaptation of technological developments from digital 4.0 to society 5.0 forces humans to have three main abilities that need to be possessed (namely creativity, critical thinking, communication and collaboration) [1]. This is because society 5.0 was initiated by the Japanese state. This concept allows us to use modern science-based (AI, Robot, and Internet of Things) for human needs with the aim that humans can live comfortably [2]. Society 5.0 was inaugurated 2 years ago, on January 21, 2019, and was made as a resolution to the industrial 4.0 resolution [3].

The main problem faced by humans today is the transition of clean energy to a net-zero emission condition [4]. The condition of Net Zero Emission necessitates the massive development of renewable energy [5]. One of the renewable energies with the

*Corresponding author: andrigunawan19240@gmail.com

Tr Ren Energy, 2022, Vol.8, No.2, 107-118. doi: 110.17737/tre.2022.8.2.00143

greatest electrical efficiency is wind power generation [6]. A wind power plant is a generator that utilizes wind pressure at a high enough speed to drive a turbine to produce electrical energy. However, its development is limited due to its intermittent nature due to changes in wind direction and wind circulation, thus requiring accurate prediction of wind circulation patterns in an area, especially in borderline, remote and less developed areas of Indonesia [7].

Indonesia is a country traversed by the equator and surrounded by two oceans and two continents. This position makes Indonesia a region that has a tropical climate [8]. Climate is a natural habit driven by a combination of factors such as solar radiation, temperature, humidity, rainfall, air temperature, air pressure and wind pressure [9]. One of the border areas in Indonesia is the province of East Nusa Tenggara [10].

The development of infrastructure in border areas must be increased for the sake of sustainability and equal human rights [11]. Apart from that, the use of radar and military operations for guarding the border areas must be fully supported by the availability of energy [12]. Therefore, wind speed prediction is needed to drive turbines from windmills to produce electrical energy [13]. However, the changing wind speed causes the efficiency of the electrical energy produced to decrease [14]. Climate change in the world has many impacts on changes in wind speed patterns [15]. For that, we need a method that can predict wind speed based on wind speed patterns that occur after climate change. Renewable energy development is accelerating with accurate information about how much wind speed will occur in East Nusa Tenggara in a certain period.

One of the machine learning methods that make predictions based on patterns in the available data is the backpropagation neural network method [16-20]. The Backpropagation Neural Network Algorithm (BPNN) is a supervised learning algorithm consisting of a perceptron with several layers to change the weights associated with the neurons in the hidden layer [21]. The principle of the Backpropagation Neural Network Algorithm can be seen in Figure 1. The backpropagation algorithm utilizes the output error to change/improve the weight value in the backward direction. Attempts to get the initial error by skipping the previous forward propagation.

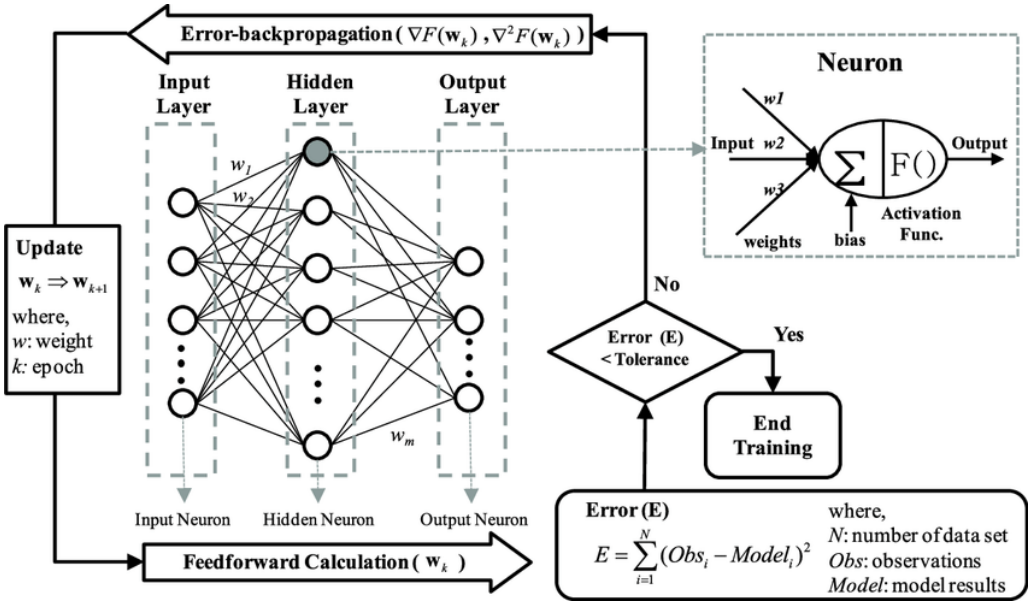


**Figure 1.** Diagram of Backpropagation Neural Network Algorithm [22]

## Data Source and Methods

Overall wind speed range data from January 2003 to December 2020 is taken from "https://power. larc.nasa.gov/data-access-viewer/" (NASA Power Data) with a point location of Latitude -8.6048 and Longitude 121.1418 in East Nusa Tenggara, Republic of Indonesia. The training data used in this study is from January to December 2003-2015, while validation uses data from January-December 2016-2020.

### Backpropagation Neural Network (BPNN) Method

The Backpropagation Neural Network (BPNN) method was originally introduced by Paul Werbos in 1974, then re-admitted by Rumelhart and McCelland in 1986 [23]. In the BPNN algorithm, network architecture uses a multilayer network. Basically, the BPNN architecture consists of three layers, namely the input layer, hidden layer and output layer. For the input layer, there is no computational process, but at the input layer, the input signal is sent to the hidden layer [24]. In the hidden and output layers, there is a computation process on the weights and biases and the magnitude of the output from the hidden and output layers is calculated based on certain activation functions. Meanwhile, the activation function usually uses binary sigmoid with the output value 0-1 [25-26]. The BPNN flowchart can be seen in Figure 2

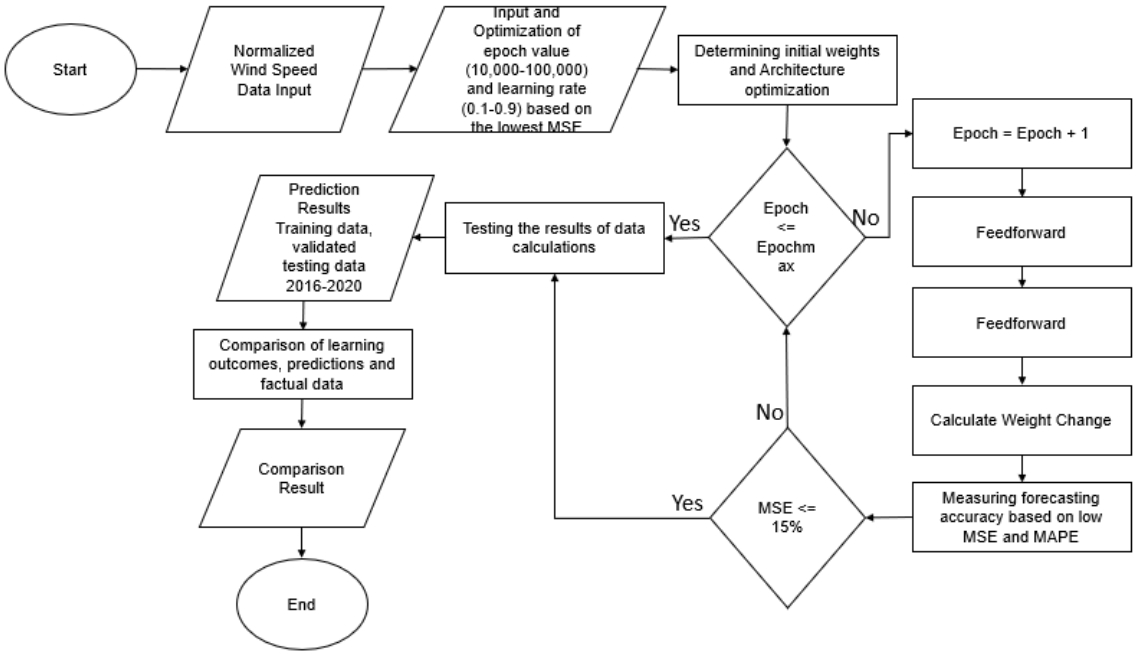


**Figure 2.** Flowchart Backpropagation Neural Network

The steps that need to be taken for BPNN training are:

1. Initialize weights with small random values.
2. As long as the stop condition is not met, do steps 3 – 8

*Step 1: Feedforward*

3. Each input unit ($xi$, =1,.....,$n$) receives the input signal $xi$ and is forwarded to the hidden layer units.

4. Each hidden unit ($zj$, =1,.....,$p$) adds up the weight of the input signal by equation (1).

$$Z_{in_{jk}} = v_{0f} + \sum_{i=1}^{n} x_i v_{ij} \quad (1)$$

where Z are hidden neurons; $v_{0f}$ is the bias weight neuron of the $j$; $x_i$ input neuron for $i$; and $v_{ij}$ input is the weight of the input neuron to the hidden neuron.
The application of the activation function is calculated by equation (2).

$$Z_j = f(Zin_j) \quad (2)$$

where $Z_j$ is unit for -$j$ in the hidden layer; and $Z_{inj}$ is the output for $Z_j$ unit. For example, the activation function used is sigmoid with equation (3).

$$Y = f(x) = \frac{1}{1+e^{-x}} \quad (3)$$

The sigmoid activation function sends this signal to all units on the output unit.

5. Each output unit ($yk$, = 1,.....,) adds a weighted input signal using equation (4).

$$Y_{in_k} = w_{0k} + \sum_{k=1}^{p} z_j w_{jk} \quad (4)$$

where $Y_{in_k}$ is output for $yk$ unit; $w_{0k}$ is bias weight for hidden neurons for-$k$; $Z_j$ is unit for-$j$ in hidden layer; and $w_{jk}$ is hidden neuron weights to output neurons.
By applying the activation function calculated by equation (5).

$$Y_k = f(Yin_k) \quad (5)$$

where $Y_{in_k}$ is output fot $Y_k$ unit.

*Step 2: Backward*

6. Each output unit ($yk$, =1,.....,$m$) receives its input training pattern. Calculate the error (error) for each layer with equation (6).

$$\delta_k = (t_k - y_k) f'(y_{in_k}) \quad (6)$$

where $\delta_k$ is a correction factor of $w_{jk}$; $t_k$ is target; $y_k$ is output neuron for k; and $y_{ink}$ is output fot $y_k$ unit.
Calculate the weight and bias correction using equation (7).

$$\Delta w_{jk} = \alpha \delta_k x_j \quad (7)$$

$$\Delta w_{jk} = \alpha \delta_k$$

where $\Delta w_{jk}$ = is the difference between $w_{jk}$ ($t$) with $w$($t$+1); $\Delta w_{0k}$ is the weight of bias for is hidden $k$; $\alpha$ is a learning rate; $\delta_k$ is the weight correction factor $w_{jk}$; and x is the input.

7. Each hidden unit ($zj$, =1,.....,) adds up its input delta (from the units in its upper layer) with equation (8).

$$\delta_{in_j} = \sum_{k=1}^{p} \delta_k w_{jk} \quad (8)$$

where the $\delta_k$ is the correction factor of $w_{jk}$; and $w_{jk}$ is the weight of neurons hidden to the output neuron. Calculate the error (error) for each layer with equation (9).

$$\delta_j = \delta_{in_j} f(x_{in_j}) \quad (9)$$

where $\delta j$ is the correction factor of $vij$; $\delta_{inj}$ is the correction factor; $x$ are inputting. Calculate the weight and bias correction with equation (10).

$$\Delta v_{ij} = \alpha \delta_j x_i \quad (10)$$

where $\Delta v_{ij}$ is the weight of the input neuron to the hidden neuron; $\alpha$ is learning rate; $\delta_j$ is the weight correlation factor $v_{ij}$; and $x_i$ is neuron input for $i$.

*Step 3: Update Weight*

8. Each output unit ($yk$, =1,.....) updates the weight, and bias ($j$ = 0.1,..$p$) is calculated by equation (11).

$$w_{jk}(new) = w_{jk}(initial) + \Delta w_{jk} \quad (11)$$

where $w_{jk}$ is the weight of hidden neurons to output neurons; and $\Delta w_{jk}$ is the difference between the weights of the hidden neurons and the output neurons. Each hidden unit ($zj$, = 1,…) updates the weight, and its bias ($i$ = 0.1,..$n$) is calculated by equation (12).

$$v_{ij}(new) = v_{ij}(initial) + \Delta v_{ij} \quad (12)$$

where $v_{ij}$ is the weight of the input neuron to the hidden neuron; and $\Delta v_{ij}$ is the difference in the weights of the input neurons to the hidden neurons.

9. Maximum input epoch will stop automatically

## Forecast Accuracy

The Validation stage in BPNN serves to measure the accuracy of the resulting learning using the Mean Squared Error (MSE) method. Data Validation also aims to find forecasting errors in each period. The measurement of accuracy will later be divided by the number of forecasting periods that have been used [27]. The formula for calculating the MSE accuracy measurement can be seen in equation (13).

$$MSE = \frac{1}{n} \sum_{i=1}^{n} (r_i - \hat{r}\, i)^2 \quad (13)$$

where $Yi$ is factual value, $\hat{r}_i$ is prediction value and n is number of periods or targets.

In particular, the determination of the best architectural optimization indicator is determined by the Mean Absolute Percentage Error (MAPE) value [28]. MAPE is a measure of predictive variation for forecasting methods in statistics, usually serveing to reveal the accuracy of the ratio determined by equation (14)

$$MAPE = \frac{100\%}{n} \sum_{i=1}^{n} \left| \frac{A_t - F_t}{A_t} \right| \quad (14)$$

*A. Data Sample*

The wind speed data used were a total of 216 datasets obtained from NASA from January 2003 to December 2020. It should be noted that January 2003 to December 2010 data is positioned as input data and the data from January 2011-December 2015 is used as training target. Validation data is determined from January 2016-December 2020. Each data set is normalized within a range of 0.1-0.9 using the equation (15) [29] with the results of data normalization shown in Tables 1 and 2 and Figure 3.

$$X' = \frac{0.8(X-b)}{(a-b)} + 0.1 \quad (15)$$

The value of X' is the normalized data, a is the maximum value of factual data, b is the minimum value of factual data, and X is factual data. Next, the prediction calculation process is carried out using the BPNN algorithm. Prediction results are denormalized to get the predicted results to their original form. The formula for calculating the denormalization of the data is equation (16) [30].

$$X = \frac{(X'-0.1)(b-a)+0.8a}{0.8} \quad (16)$$

**Table 1.** Wind speed of 2011-2015 period actual (Learning)

| Month | Year (m/s in normalization scale) | | | | |
|---|---|---|---|---|---|
| | 2011 | 2012 | 2013 | 2014 | 2015 |
| January | 0.625444 | 0.716737 | 0.868216399 | 0.632883 | 0.639645 |
| February | 0.53415 | 0.616653 | 0.638968724 | 0.597718 | 0.52874 |
| March | 0.546999 | 0.745139 | 0.487489434 | 0.549028 | 0.457735 |
| April | 0.448267 | 0.388757 | 0.657227388 | 0.42798 | 0.448267 |
| May | 0.491547 | 0.691716 | 0.500338123 | 0.470583 | 0.509129 |
| June | 0.454353 | 0.499662 | 0.557819104 | 0.385376 | 0.42798 |
| July | 0.451648 | 0.537532 | 0.474640744 | 0.526036 | 0.534827 |
| August | 0.427303 | 0.499662 | 0.44353339 | 0.434742 | 0.410397 |
| September | 0.450972 | 0.484108 | 0.525359256 | 0.555114 | 0.473288 |
| October | 0.438123 | 0.397549 | 0.509129332 | 0.534827 | 0.557819 |
| November | 0.39011 | 0.391462 | 0.473964497 | 0.407692 | 0.417836 |
| December | 0.511158 | 0.409045 | 0.634911243 | 0.503719 | 0.608538 |

**Table 2.** Wind speed of 2016-2020 period actual (Validate)

| Month | Year (m/s in normalization scale) | | | | |
|---|---|---|---|---|---|
| | 2016 | 2017 | 2018 | 2019 | 2020 |
| January | 0.60989 | 0.574725 | 0.80262 | 0.834404 | 0.722147 |
| February | 0.628825 | 0.769484 | 0.561877 | 0.605156 | 0.590279 |
| March | 0.430685 | 0.522654 | 0.632883 | 0.70727 | 0.448267 |
| April | 0.362384 | 0.461116 | 0.473288 | 0.470583 | 0.521302 |
| May | 0.509806 | 0.384024 | 0.397549 | 0.504396 | 0.549028 |
| June | 0.507101 | 0.384024 | 0.464497 | 0.461792 | 0.40093 |
| July | 0.569315 | 0.527388 | 0.498309 | 0.415131 | 0.457058 |
| August | 0.537532 | 0.526036 | 0.553085 | 0.540237 | 0.511158 |
| September | 0.493576 | 0.496957 | 0.490194 | 0.436095 | 0.416484 |
| October | 0.43339 | 0.507777 | 0.469907 | 0.487489 | 0.480727 |
| November | 0.398901 | 0.451648 | 0.439476 | 0.362384 | 0.484784 |
| December | 0.695773 | 0.511834 | 0.509129 | 0.461116 | 0.533474 |

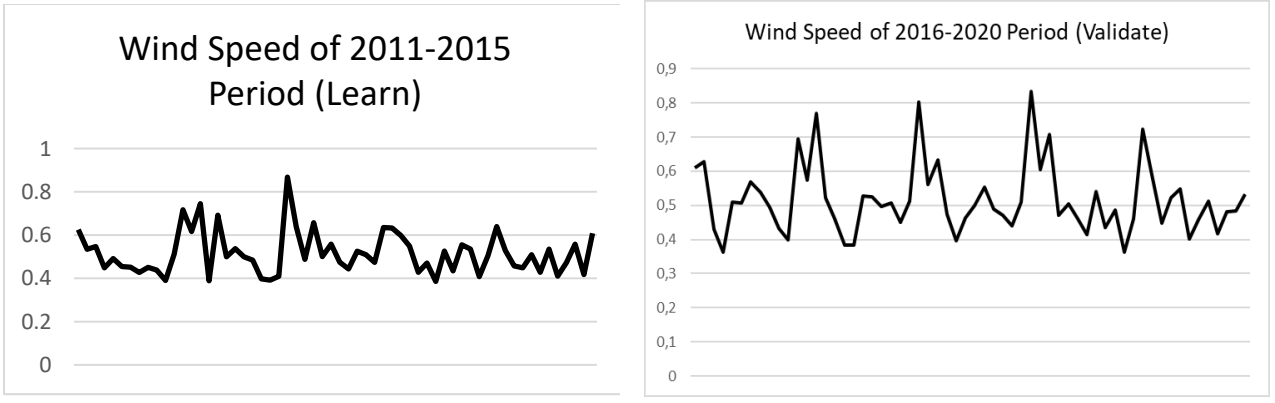


(a) (b)

**Figure 3.** (a) Graph of wind speed for the period 2011-2015 Factual (Learn) (b) Graph of wind speed for the period 2016-2020 Factual (Validate)

## Results and Discussion

Wind speed predictions have been made from 2016-2020, and the data is generated from the optimization process to get the best learning rate and epoch. Learning rate and epoch are said to have the most ideal values when the resulting MSE parameter

is very small. Therefore, optimization is carried out utilizing an input learning rate from 0.1-0.9. The number of epochs further optimized from 100 to 1000 with a step of 100. If the resulting accuracy is still low, the optimization is increased by the number of epochs from 1000 to 10,000 with a step of 1000. If the MSE accuracy still does not meet, then re-optimize the epoch value from 10,000 to 100,000 with Steps 10,000 (to get the best MSE score). The graph of the relationship between epoch optimization and learning rate on the MSE value is shown in Figure 4.

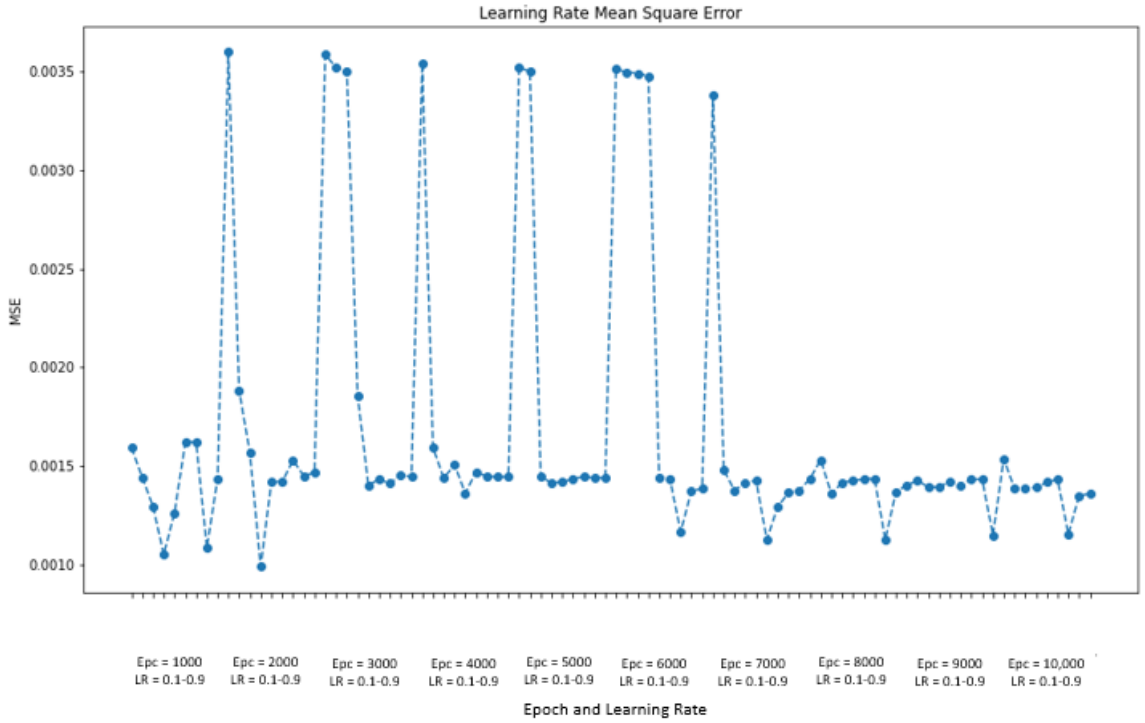


**Figure 4.** Graph of the relationship between epoch value and learning rate on MSE

Based on Figure 4, it can be seen that the distribution of the best epoch values and learning rate is based on the lowest MSE value. Figure 4 shows that the lowest MSE value is only 0.0001% (below 0.0010%) with the best learning rate parameter of 0.4 and the best epoch value is 20,000. This is the same as the parameter reported by Rozycki *et al.* [31]. However, the epoch and learning rate parameter values are not necessarily universally applicable to all data, but only applies to certain datasets. Therefore, before making predictions, it is better to optimize learning rate and epoch, which is the same as reported by Wanto *et al.* [32]. If all the best optimization parameters are obtained, then predictions are made using the BPNN method to produce the values in Table 3.

It can be seen that BPNN learning-prediction predicts the information/parameters from Layer, Epoch, Learning rate, MSE and MAPE as a whole during the learning process and validation process.The results of the optimization of the architectural model at the learning stage are 8-7-5, the learning rate is 0.4, and the epoch is 20,000. The model has obtained very good accuracy with MSE = 0.000552 and MAPE = 2.942524. These parameters can also predict validation data from 2016-2020 with fairly good accuracy with MSE Validate values = 0.00903 and MAPE Validate = 14.3468. This result is an ideal value, because the MAPE value is below 15%. This is following what was reported by Okumus *et al.* [33]. So, the learning process has met the requirements for

use in the prediction process. But further optimization is needed for the prediction process, because the prediction stage is the most important stage for predicting wind speed patterns that may occur in East Nusa Tenggara.

**Table 3.** Best parameters of prediction wind speed with BPNN

| Variable Result | Type | Value | | |
|---|---|---|---|---|
| | | Hidden Layer | Neuron Hidden Layer | Architectures |
| Layer | Learning | 1 | 7 | 8-7-5 |
| | Prediction | 2 | 11 5 | 8-11-5-5 |
| Epoch and Learning Rate | Learning | 20,000 and 0.4 | | |
| | Prediction | 20,000 and 0.4 | | |
| MSE (%) | Learning | 0.000552 | | |
| | Prediction | 0.001416 | | |
| MAPE (%) | Learning | 2.942524 | | |
| | Prediction | 5.982144 | | |
| Validate MSE (%) | Learning | 0.00903 | | |
| | Prediction | 0.007634 | | |
| Validate MAPE (%) | Learning | 14.3468 | | |
| | Prediction | 11.62783 | | |

Based on Table 3, the data prediction process produces the best parameters with an 8-11-5-5 architectural model, a learning rate of 0.4 and 20,000 epochs. The best parameter is calculated based on the lowest value of MSE = 0.001416% and MAPE = 5.982144%. This value is quite large when compared to the results of the learning process. The learning architecture model (8-7-5) and predictions (8-11-5-5) have very low MSE and MAPE values, but these values are not absolute for data validation cases. This is indicated by the value of each MSE and MAPE which increases in the validation case. The Prediction Architecture Model has a relatively small accuracy of Validate MSE and Validate MAPE values of 0.007634 and 11.62783, respectively. When compared to the learning model, the predictive architectural model (8-11-5-5) is much more predictable than learning architecture (8-7-5). The accuracy is acceptable. this is relevant to the validated MSE and MAPE values reported by Saputra *et al.* [34]. The comparison graph between the best architecture for the learning process and the best architectural model for the prediction process against the actual/target value is shown in Figure 5.

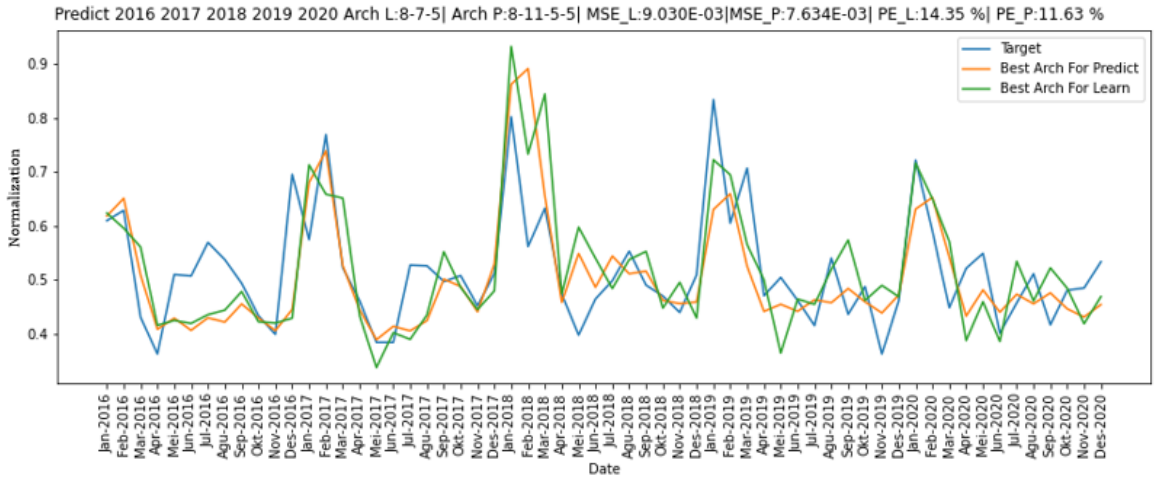

**Figure 5.** Graph of All Predict Process 2016-2020 (-- = Actual data/Target), (-- = 8-7-5/Best Architecture for learn), and (-- = 8-11-5-5/Best Architecture for predict)

Based on Figure 5, it can be seen that the blue line is the actual/target data, the green line is the learning data (the best Learning Architecture Model) and the yellow line is the predictive data (the best Prediction Architecture Model). The figure shows that the predicted wind speed pattern and learning have followed the actual/target data pattern that occurred in the field. The biggest deviation occurred in April 2016-August 2016. The large deviation in the learning model and predictions has the potential to be caused during the learning data process in 2011-2015 as shown in Figure 3(a). It can be seen that there is no peak or increase in wind speed data at the beginning of the graph pattern. So during validation, just comparing the data (where there is no learning process) leads to a sufficiently large deviation, but still tolerable. Therefore, it can be seen that an unusual natural phenomenon occurred because it disrupted the wind speed pattern from the year before and after.

Based on a report from the Kupang Meteorology, Climatology and Geophysics Agency stating the potential for natural phenomena that may occur in the East Nusa Tenggara region, every season transition is always interspersed with strong winds reaching 55 km/hour and rain with light to moderate intensity. In the Australian monsoon, there is movement the east-southeast wind to pass through East Nusa Tenggara once every two weeks, especially in June and July, even until August of the current year. However, this year, due to high climate deviations, the impact began to be felt in May and generally the Australian monsoon brings dry winds or heat from southern Australia to East Nusa Tenggara [35]. The results of the 2016-2020 wind speed prediction using the 8-11-5-5 architectural model are shown in Table 4.

**Table 4.** Wind Speed of 2016-2020 Prediction Denormalization Data (Validate)

| Month | Year | | | | |
|---|---|---|---|---|---|
| | 2016 (m/s) | 2017 (m/s) | 2018 (m/s) | 2019 (m/s) | 2020 (m/s) |
| January | 7.03725877 | 7.880751271 | 10.3559324 | 7.201820081 | 7.213083189 |
| February | 7.483151795 | 8.678004264 | 10.75178206 | 7.598292216 | 7.504696284 |
| March | 5.55199223 | 5.790933574 | 7.541137783 | 5.771525779 | 5.996668358 |
| April | 4.185202364 | 4.678376886 | 4.863762873 | 4.635143496 | 4.516272922 |
| May | 4.463298459 | 3.921113849 | 6.092103254 | 4.812364779 | 5.175955238 |
| June | 4.159088526 | 4.259921358 | 5.242626127 | 4.636795741 | 4.614035022 |
| July | 4.473087999 | 4.146567424 | 6.027708108 | 4.928017121 | 5.066550994 |
| August | 4.36522963 | 4.401729795 | 5.583364054 | 4.854122467 | 4.827021693 |
| September | 4.822082341 | 5.448518907 | 5.647863928 | 5.210321353 | 5.101519002 |
| October | 4.466720284 | 5.264611714 | 4.912645469 | 4.875180557 | 4.699240739 |
| November | 4.15191332 | 4.624395073 | 4.831298121 | 4.596285319 | 4.494179964 |
| December | 4.684534993 | 5.832190394 | 4.871558433 | 5.047697892 | 4.805826726 |

## CONCLUSIONS

Wind speed prediction analysis in East Nusa Tenggara Province using the Backpropagation Neural Network (BPNN) method has been implemented. Based on the results of the approach, the BPNN method divides the Learning Phase from the January 2011-December 2015 data and the Validation Phase on the January 2016-December 2020 data. The best predictive architecture model is 8-11-5-5, the learning rate is 0.4 and the

epoch is 20,000. The prediction accuracy is very good with MSE Validate value of 0.007634 and MAPE Validate of 11.62783. The highest wind speed was shown in February 2018 as 10.75 m/s. Therefore, the BPNN method can be an alternative in predicting wind speed in East Nusa Tenggara Province, so that it can be taken into consideration in building wind power plants. Future work can use other prediction methods to increase the confidence of the current predictive value.

## ACKNOWLEDGMENTS

This research was supported and funded by Indonesia Defense University, Faculty of Defense Management, Department of Energy Security.

## CONFLICTS OF INTEREST

The authors declare that there is no conflict of interests regarding the publication of this paper.

## REFERENCES

[1] Mujiono, M. N. (2021). The Shifting Role of Accountants in the Era of Digital Disruption. *International Journal of Multidisciplinary: Applied Business and Education Research*, 2(11), 1259-1274.
[2] Önday, Ö. (2020). Society 5.0-its historical logic and its structural development. *Journal of Scientific Reports*, 2(1), 32-42.
[3] Achmad, W. (2021). Citizen and Netizen Society: The Meaning of Social Change From a Technology Point of View. *Jurnal Mantik*, 5(3), 1564-1570.
[4] Oshiro, K., Masui, T., and Kainuma, M. (2018). Transformation of Japan's energy system to attain net-zero emission by 2050. *Carbon Management*, 9(5), 493-501.
[5] Cassarino, T. G., and Barrett, M. (2022). Meeting UK heat demands in zero emission renewable energy systems using storage and interconnectors. *Applied Energy*, 306, 118051.
[6] Washburn, C., and Pablo-Romero, M. (2019). Measures to promote renewable energies for electricity generation in Latin American countries. *Energy Policy*, 128, 212-222.
[7] Albadi, M. H., and El-Saadany, E. F. (2010). Overview of wind power intermittency impacts on power systems. *Electric power systems research*, 80(6), 627-632.
[8] Malik, N. Y. (2019). Visual landscape analysis of coastal tourism potential in Geopark Ciletuh-Palabuhanratu Indonesia. *Scientific Bulletin" Mircea cel Batran" Naval Academy*, 22(2), 46A-52.
[9] Körner, C. (2007). The use of ‘altitude’in ecological research. *Trends in Ecology & Evolution*, 22(11), 569-574.
[10] Paulus, C. A., Azmanajaya, E., Pellokila, M. R., and Paranoan, N. (2020, February). Prospective strategies for sustainable local economic development in support of the SDGs’ goals “inclusive and sustainable economic growth” in the border region of

Indonesia–Timor Leste, Belu Regency, East Nusa Tenggara Province, Indonesia. In *Journal of Physics: Conference Se*ries (Vol. 1464, No. 1, p. 012053). IOP Publishing.
[11] Kotzé, L. J. (2014). Human rights and the environment in the Anthropocene. *The Anthropocene Review*, 1(3), 252-275.
[12] Vadivelan, N., Taware, M. S., Chakravarthi, M. R. R., Palagan, C. A., and Gupta, S. (2021). A border surveillance system to sense terrorist outbreaks. *Computers & Electrical Engineering*, 94, 107355.
[13] Kusiak, A., Zhang, Z., and Verma, A. (2013). Prediction, operations, and condition monitoring in wind energy. *Energ*y, 60, 1-12.
[14] Dai, J., Yang, X., Hu, W., Wen, L., and Tan, Y. (2018). Effect investigation of yaw on wind turbine performance based on SCADA data. *Energy*, 149, 684-696.
[15] Rasmussen, D. J., Holloway, T., and Nemet, G. F. (2011). Opportunities and challenges in assessing climate change impacts on wind energy—a critical comparison of wind speed projections in California. *Environmental Research Letters*, 6(2), 024008.
[16] Brahimi, T. (2019). Using artificial intelligence to predict wind speed for energy application in Saudi Arabia. *Energie*s, 12(24), 4669.
[17] Khosravi, A., Machado, L., and Nunes, R. O. (2018). Time-series prediction of wind speed using machine learning algorithms: A case study Osorio wind farm, Brazil. *Applied Energy*, 224, 550-566.
[18] TASDEMİR, S., YANİKTEPE, B., and burak GUHER, A. (2018). The effect on the wind power performance of different normalization methods by using multilayer feed-forward backpropagation neural network. *International Journal of Energy Applications and Technologies*, 5(3), 131-139.
[19] Kulkarni, P. A., Dhoble, A. S., and Padole, P. M. (2019). Deep neural network-based wind speed forecasting and fatigue analysis of a large composite wind turbine blade. *Proceedings of the Institution of Mechanical Engineers, Part C: Journal of Mechanical Engineering Science*, 233(8), 2794-2812.
[20] Sun, W. and Wang, Y. (2018). Short-term wind speed forecasting based on fast ensemble empirical mode decomposition, phase space reconstruction, sample entropy and improved back-propagation neural network. *Energy conversion and Management*, 157, 1-12.
[21] Mia, M. M. A., Biswas, S. K., Urmi, M. C., and Siddique, A. (2015). An algorithm for training multilayer perceptron (MLP) for Image reconstruction using neural network without overfitting. *International Journal of Scientific & Technology Research*, 4(02), 271-275.
[22] Kim, S. E. and Seo, I. W. (2015). Artificial Neural Network ensemble modeling with conjunctive data clustering for water quality prediction in rivers. *Journal of Hydro-Environment Researc*h, 9(3), 325-339.
[23] Mislan, M., Haviluddin, H., Hardwinarto, S., Sumaryono, S., and Aipassa, M. (2015, August). Rainfall monthly prediction based on artificial neural network: a case study in Tenggarong Station, East Kalimantan-Indonesia. *The International Conference on Computer Science and Computational Intelligence* (ICCSCI 2015)-Procedia Computer Science 59.
[24] Karsoliya, S. (2012). Approximating number of hidden layer neurons in multiple hidden layer BPNN architecture. *International Journal of Engineering Trends and Technology*, 3(6), 714-717.

[25] Sharma, S., Sharma, S., and Athaiya, A. (2017). Activation functions in neural networks. *Towards Data Science*, 6(12), 310-316.
[26] Asaad, R. R. and Ali, R. I. (2019). Back Propagation Neural Network (BPNN) and sigmoid activation function in multi-layer networks. *Academic Journal of Nawroz University*, 8(4), 216-221.
[27] Alfred, R. (2015, October). A genetic-based backpropagation neural network for forecasting in time-series data. In *2015 International Conference on Science in Information Technology (ICSITech)* (pp. 158-163). IEEE.
[28] Bai, Y., Li, Y., Wang, X., Xie, J., and Li, C. (2016). Air pollutants concentrations forecasting using back propagation neural network based on wavelet decomposition with meteorological conditions. *Atmospheric Pollution Rese*arch, 7(3), 557-566.
[29] Eesa, A. S. and Arabo, W. K. (2017). A normalization methods for backpropagation: a comparative study. *Science Journal of University of Zakho*, 5(4), 319-323.
[30] Wang, H. S., Wang, Y. N., and Wang, Y. C. (2013). Cost estimation of plastic injection molding parts through integration of PSO and BP neural network. *Expert Systems with Applications*, 40(2), 418-428.
[31] Rozycki, P., Kolbusz, J., Krzos, G., and Wilamowski, B. M. (2019, April). Approximation-based Estimation of Learning Rate for Error Back Propagation Algorithm. In *2019 IEEE 23rd International Conference on Intelligent Engineering Systems (INES)* (pp. 000065-000070). IEEE.
[32] Wanto, A., Zarlis, M., and Hartama, D. (2017, December). Analysis of Artificial Neural Network Backpropagation Using Conjugate Gradient Fletcher Reeves in the Predicting Process. In *Journal of Physics: Conference Series* (Vol. 930, No. 1, p. 012018). IOP Publishing.
[33] Okumus, I. and Dinler, A. (2016). Current status of wind energy forecasting and a hybrid method for hourly predictions. *Energy Conversion and Management*, 123, 362-371.
[34] Saputra, W., Hardinata, J. T., and Wanto, A. (2020). Resilient method in determining the best architectural model for predicting open unemployment in Indonesia. In *IOP Conference Series: Materials Science and Engineer*ing (Vol. 725, No. 1, p. 012115). IOP Publishing.
[35] PCN. (2016). BMKG Kupang: NTT Sedang Musim Peralihan. https://www.beritasatu.com/nasional/364945/bmkg-kupang-ntt-sedang-musim-peralihan (accessed on 4/9/2022).



Trends in Renewable Energy
OPEN ACCESS ISSN: 2376-2144
Peer-Reviewed Article futureenergysp.com/index.php/tre

# A Review of the Effect of Compressed Natural Gas (CNG) on Combustion and Emission Performance of Internal Combustion Engines

Yufan Liang*

*School of Mechanical Engineering/Institute of Vehicles and New Energy Technology, North China University of Water Resources and Electric Power, Zhengzhou City, Henan, China*

Received April 24, 2022; Accepted June 21, 2022; Published July 9, 2022

In order to reduce the environmental pollution caused by conventional internal combustion engines, the application of natural gas in internal combustion engines and the combustion and emission performance of natural gas internal combustion engines have been widely studied by scholars. Because the physical and chemical properties of natural gas are different from those of conventional gasoline or diesel, the operating performance of natural gas internal combustion engines in practical applications is also different from that of conventional internal combustion engines. This paper presents the physicochemical properties of compressed natural gas, the two combustion modes (premixed combustion and non-homogeneous diffusion combustion) in internal combustion engines and the effect of compressed natural gas on the performance of internal combustion engines. Compared with gasoline engines, natural gas internal combustion engines have relatively lower power and higher effective power loss; lower effective fuel consumption rate in terms of economy; and lower CO and $NO_x$ emissions than gasoline engines in terms of emissions.

*Keywords: Clean Energy; Compressed Natural Gas (CNG); Combustion and Emission Performance; Improvement Methods*

## Introduction

Globally, 95% of transportation energy comes from fossil fuels [1-2]. To solve the energy crisis and reduce the environmental pollution caused by vehicle emissions, many countries are actively searching for alternative energy sources. The availability and environmental friendliness of compressed natural gas (CNG) as a clean energy source make it a preferred alternative fuel in internal combustion engines, and the application of natural gas in spark ignition (SI) and compression ignition (CI) engines has been widely studied.

The main component of natural gas is methane ($CH_4$) at 60 to 90%, which is followed by various other hydrocarbons. Compared with gasoline, there are certain deficiencies in automotive applications. To improve the performance of natural gas engines, many scholars have studied the combustion and emission performance of natural gas engines. Kontses *et al.* [3] conducted tests on diesel, gasoline, liquefied petroleum gas (LPG), and compressed natural gas (CNG) vehicles for particulate emissions. It was

**Corresponding author:* 1602399186@qq.com

Tr Ren Energy, 2022, Vol.8, No.2, 119-129. doi: 110.17737/tre.2022.8.2.00144

found that diesel and CNG engines had the lowest emissions with PN (number of particles) values as low as $7.8\times10^{9}$ and $2.4\times10^{10}$ p/km, respectively. Yontar and Doğu [4] investigated the effect of gasoline and CNG fuels on the low and high load conditions of a two-phase relay ignition engine and showed that CNG reduced the maximum torque by 15.6 % and 19.6 % at a throttle opening of 75 % and 25 %, respectively, compared to gasoline. Overall, the use of CNG reduced the emissions of $CO_2$ and HC, but engine performance parameters such as torque and power were reduced. By studying the effect and optimization of EGR on natural gas engines, Guo *et al.* [5] concluded that exhaust gas recirculation (EGR) fluctuations in the intake manifold lead to differences in the EGR rate entering each cylinder during the intake process, and optimization can reduce the differences. Tahir *et al.* [6] selected a single cylinder spark ignition (SI) engine to study the effect of CNG on spark ignition engine, and showed that the in-cylinder pressure of CNG is 20% lower than that of gasoline. Liu *et al.* [7] improved the intake pipe to solve the problem of poor uniformity of natural gas engine operation. Han *et al.* [8] designed a new spark ignition compressed natural gas (CNG) engine and studied the combustion performance. The results showed that the torque of CNG engine increased from 5.2 % to 6.6 % when the compression ratio increased from 10.5 to 12, and increasing the compression ratio could improve the performance of CNG to some extent. Sahoo and Srivastava [9] studied the effect of compression ratio on effect of engine burst, performance, combustion and emission characteristics of dual-fuel CNG engine. The results showed that the peak burst of gasoline engine was significantly higher than that of CNG engine, and the fuel consumption and thermal efficiency of CNG were improved at higher speed compared to gasoline engine.

The performance of a natural gas engine depends mainly on the actual working process. The combustion process of the fuel entering the cylinder directly affects the thermal power conversion rate and exhaust gas composition of the engine, so the improvement of engine performance cannot be achieved without the improvement of the engine combustion process. This paper reviews the effect of compressed natural gas (CNG) fuel on the performance of internal combustion engines from the perspective of combustion and emission.

## Physical and Chemical Properties of Natural Gas

Natural gas, as the first alternative fuel for vehicles implemented in China, has been widely used in public transportation in some cities with its favorable price and obvious emission reduction effect [10]. The basic physicochemical properties of natural gas are different from those of traditional gasoline diesel. As a gaseous fuel, its octane number is significantly higher than that of gasoline, and it shows a blue flame during combustion. The basic physicochemical properties of natural gas are as follows.

(1) Density. The density of natural gas is 0.78 kg/m$^3$ at atmospheric pressure, which is less than the density of air (1.293 kg/m$^3$).

(2) Low calorific value. The low calorific value of natural gas by mass is 50.0 MJ/kg, which is higher than the low calorific value of gasoline (43.9 MJ/kg). However, the theoretical mixture calorific value of natural gas is 3.39 MJ/m$^3$, which is lower than that of gasoline engine (3.73 MJ/m$^3$). So the theoretical mixture calorific value of natural

gas is relatively low.

(3) Boiling point. The boiling point of natural gas is -162℃, which is not easily liquefied and usually exists in a gaseous form.

(4) Ignition temperature. The ignition temperature of natural gas is about 537℃, which is significantly higher than the ignition temperature of gasoline (390~420 ℃). Therefore, when natural gas is used in engines, it is easy to use the ignition method due to its higher ignition temperature, and not suitable for the compression ignition mode.

(5) Octane number. Octane number is proportional to the explosive resistance. The octane number of natural gas is about 120, which is higher than that of gasoline (90 ~ 98). So, it has good anti-explosive performance, and is suitable for higher compression ratios.

(6) Ignition limit. The volume concentration of natural gas ignited in air ranges from 5% to 15%, and the calculated excess air coefficient ranges from 0.6 to 1.8. Therefore, the lean burn of natural gas in an internal combustion engine can improve its economy.

A comparison of the physical and chemical properties of natural gas, gasoline and diesel is given in Table 1 [11].

**Table 1** Comparison of physical and chemical properties of natural gas with gasoline and diesel

| Fuel | Mass fraction | Density/(kg·m$^{-3}$) | | Theoretical air-fuel ratio | |
|---|---|---|---|---|---|
| | | Gas phase | Liquid phase | Volume ratio | Quality ratio |
| Natural Gas | C:75 H:25 | 0.715 | 424 | 9.5 | 17.3 |
| Gasoline | C:85 H:15 | — | 720-737 | 8586.0 | 14.7 |
| Diesel | C:86 | — | 840 | 9417.0 | 14.0 |

| Low calorific value (MJ·kg$^{-1}$) | Octane Number (RON) | Cetane number (CN) | Fire limit (Volume) /% | Ignition temperature /℃ | Flame propagation rate /( cm·s$^{-1}$) |
|---|---|---|---|---|---|
| 47.6 | 108 | — | 5.0 ~15.0 | 645 | 34 ~37 |
| 43.9 | 80 ~99 | 0 ~10 | 1.3 ~7.6 | 392 ~421 | 38 ~45 |
| 42.5 | 20 ~30 | 35 ~60 | 1.5 ~8.2 | 230 | 39 ~47 |

## Combustion Methods and Characteristics of CNG in Internal Combustion Engines

With the continuous development and progress in the automotive field, compressed natural gas is more widely used in automobiles. According to the classification of CNG fuel supply method, the combustion method of CNG internal combustion engine can be divided into two types: premixed combustion type and non-homogeneous diffusion combustion type.

## Pre-mixed Combustion Type

*Hybrid Gas Formation Characteristics*

In a premixed combustion internal combustion engine, natural gas is mixed with air at the intake pipe or valve and enters the cylinder on the engine intake stroke. Before spark ignition or fuel ignition, a more homogeneous combustible mixture has formed in the cylinder.

*Combustion Characteristics*

Since the mixture in the cylinder is relatively uniform, a stable nucleus is formed by spark ignition or fuel ignition, and the mixture is burned in the form of flame propagation with the nucleus as the center. Pre-mixed combustion type natural gas engines include spark ignition and diesel-natural gas dual-fuel engine [12]. Homogeneous mixture combustion (HCCI) is a new combustion method in natural gas diesel engines. During HCCI combustion, uniformly mixed air-fuel and residual exhaust gases are compressed and ignited without any obvious flame propagation process, and the overall combustion temperature is relatively uniform [13]. In addition, spark ignition type engines with lean combustion technology can increase the average effective pressure and reduce the combustion temperature and $NO_x$ emissions [14-16]. However, at low load, it is easy for the mixture to be too lean, resulting in misfire or incomplete combustion and increased CO and HC emissions. During the combustion process of the pilot-ignition engine, the air-fuel mixture gradually becomes leaner as the load decreases. The mixture is too lean, resulting in incomplete combustion and a significant increase in HC and CO emissions, which is not suitable for medium and low load operation. Based on analysis of the combustion and emission performance of premixed combustion natural gas engines, it can be seen that the mixture is formed before spark ignition or ignition. Combustion relies mainly on flame propagation, so the mixture is relatively dense, reducing fuel economy. In addition, it also leads to greater volumetric efficiency loss of natural gas engines, reducing the output power. For example, the use of lower compression ratio to suppress deflagration will reduce the thermal efficiency of the engine at all operating conditions. Zhang *et al.* [17] improved the performance and emissions of the micro-premixed combustion mode which were compared with those in the hybrid restricted combustion mode. The results showed that the brake thermal efficiency could be improved by 1.1-3.6 % with the micro-premixed combustion mode at different loads.

## Non-Homogeneous Diffusion Combustion Type

*Hybrid Gas Formation Characteristics*

Non-homogeneous diffusion-combustion natural gas engines use in-cylinder direct injection of natural gas as the fuel supply method. In a direct injection natural gas engine, due to the lower density of natural gas compared to diesel and gasoline, the natural gas jet is still lower even with a higher jet velocity during the injection process, and the mixing velocity with air is lower. Therefore, it is more necessary to organize in-cylinder airflow moves to promote the mixing of natural gas and air.

*Combustion Characteristics*

There are two types of direct injection natural gas engines: low pressure injection and high pressure injection, and the low pressure in-cylinder injection natural gas engine is still a premixed combustion type. Non-homogeneous diffusion combustion is similar to conventional diesel combustion, allowing the gas to be burned at the same time as the injection. This method does not require much premixed combustion, keeps the pressure rise rate stable, and helps reduce $NO_x$ emissions and particulate matter emissions. Among the performance and emissions of six CNG combustion modes including homogeneous compression ignition and non-homogeneous diffusion combustion, Wang *et al.* [13] mentioned that the non-homogeneous diffusion combustion mode of diesel natural gas has good overall performance, reaching the thermal efficiency level of conventional diesel engines while reducing $NO_x$ and CO emissions. Direct in-cylinder injection (DIC) [18] is a high-pressure injection of natural gas before the compression upper stop, ignited by a small amount of diesel or an electric plug, to achieve diffusion of the non-homogeneous mixture, thus solving the problem of premixed combustion in natural gas engines. Compared with intake tract injection, direct in-cylinder injection natural gas engines can avoid the loss of volumetric efficiency and reduce the possibility of unburned hydrocarbons and deflagration.

## The Effect of CNG on the Performance of Internal Combustion Engines

Natural gas as a clean energy source has been studied for the performance of internal combustion engines mainly in terms of power, economy and emission. Many studies have been done by experts and scholars on natural gas as an alternative fuel for automotive engines. CNG is extremely vaporizable and can be quickly mixed with other work gases to form a homogeneous combustible mixture, resulting in a better combustion process and improved emission and thermal efficiency. Therefore, engines using CNG as fuel can have better power, economy and emission performance [19]. Verma *et al.* **Error! Reference source not found.** studied the effect of different EGR rates on the combustion and emission of a high-pressure direct injection (HPDI) engine by building a three-dimensional computational fluid dynamics (CFD) diesel/natural gas dual fuel injection model. Natural gas dual fuel injection model is used to study the effect of different EGR rates on the combustion and emission characteristics of high pressure direct injection (HPDI) engines. The results showed that the high-temperature region is mainly formed by the combustion of natural gas jets ignited by diesel fuel, and NO is mainly generated in the high-temperature region generated by the combustion of natural gas jets. The combustion of ignited diesel fuel contributes less to NO generation. Zheng *et al.* [22] investigated the combustion and emission characteristics and economics of a heavy-duty natural gas engine blended with different ratios of reformed gas by selecting a suitable catalytic oxidizer in a natural gas engine, and improved the performance of the natural gas engine by oxidizing the catalytic reforming system. In the literature [23], a comparison of the power and economy of natural gas internal combustion engines and gasoline engines is shown in Figures 1 and 2.

### Dynamic Characteristics

Comparing the dynamics of the natural gas internal combustion engine with the gasoline engine (as shown in Figure 1), the CNG engine is lower than the gasoline engine in power and torque experimental data, and the torque gap is the largest at 5200 r/min, which is 21.93% lower than that of the gasoline engine. At this speed, the power gap is the largest, which is 19.37%. The CNG engine has an effective power loss. The causes of effective power loss include the following:

(1) Fuel flame propagation is slow. The main component of natural gas is methane, which has the slowest flame propagation speed when burned compared to conventional fuels such as gasoline and diesel. The characteristic of natural gas combustion is that the ignition temperature is high, which makes the total combustion cycle of the natural gas engine longer, and the peak gas pressure in the cylinder deviates from the top dead center, resulting in a slow rise in the pressure and temperature in the cylinder. Therefore, CNG engines require a larger ignition advance angle compared to gasoline [24]. Increasing the ignition advance angle results in a decrease in engine power. Theoretically, a unit mass of natural gas requires more air to burn than gasoline. For an engine with the same displacement, the combustion quality of natural gas is lower than that of gasoline, resulting in lower natural gas engine power. Mixing flammable and explosive hydrogen and natural gas can speed up the combustion.

(2) Volumetric efficiency loss. The density of CNG in the gas phase is lower than that of air, and relatively less air enters the cylinder during the intake process. Whereas in a gasoline engine, gasoline does not reduce the amount of air entering the cylinders. Therefore, the output power of the gasoline engine will be better than that of the CNG engine during the combustion process. To improve the power performance of the engine, the volumetric efficiency of the CNG engine can be improved using increasing the number of intake valves per cylinder, increasing valve timing and lift optimization, and using a supercharged CNG engine.

In order to improve the power performance of natural gas engines, different percentages of reformed gas could be blended [22], and the combustion characteristics of natural gas engines showed that the peak in-cylinder pressure and the cyclic variation of IMEP (The Indicates Mean Effective Pressure) were significantly reduced and the engine ran more smoothly.

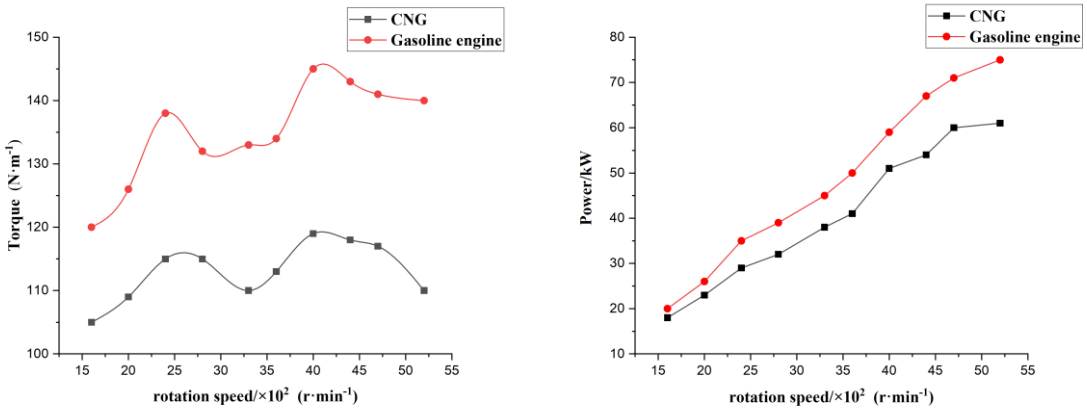


(a)Torque (b)Tower

**Figure 1.** Comparison of CNG internal combustion engine and gasoline engine dynamics

## Economic Characteristics

Economy is mainly expressed through the fuel consumption rate, where higher effective fuel consumption rate represents better economy of internal combustion engines. Due to the higher low calorific value of CNG, less fuel is consumed at the same power output compared to gasoline engines. The effective fuel consumption rate with CNG fuel is 12% to 20%, which is lower than gasoline over the entire speed range. However, for CNG/diesel engines, the fuel consumption rate is lower at medium and high loads, and the fuel consumption rate is higher at low loads. And because the combustion efficiency is low, the thermal efficiency at low load is also low. To meet its economy, the combustion rate of gas should be increased to reduce fuel consumption. Due to the low effective fuel consumption rate and high CNG calorific value, the effective thermal efficiency of natural gas engines is 5-12% higher than that of gasoline engines. CNG/diesel dual-fuel engines are more suitable for working under medium and high loads, and have higher thermal efficiency and lower fuel consumption rates under medium and high loads [25].

## Emission Characteristics

The emission performance of the engine is mainly analyzed through the control of CO, HC, NOx and solid particulate matter By comparing the emissions from burning CNG and burning gasoline (as shown in Figure 2), it can be concluded that $NO_x$ emissions from CNG and gasoline have the same trend, and $NO_x$ emissions from CNG are lower than those of gasoline at all RPMs. The $NO_x$ emission reduction at 1600r/min is the largest, which is 81.66%. For CO emissions, the CO emissions trends for both fuels are also consistent, except for 2000 r/min and 2800 r/min. The CO emissions of the CNG engine at all speeds are lower than those of the gasoline engine, with a maximum decrease of 26.67% at 3200r/min.

CNG engines have the highest hydrogen-to-carbon ratio. Hydrogen-rich natural gas (HCNG) is an emerging alternative gas fuel, which has a higher low calorific value and relatively slow flame propagation compared to gasoline, resulting in a lower maximum temperature of its combustion chamber than ordinary gasoline engines. The main factors affecting $NO_x$ emissions of a CNG engine are oxygen content, combustion temperature, etc. The longer the reaction time and the higher the temperature under adequate oxygen content, the higher the $NO_x$ emissions. The overall $NO_x$ emissions increase with the increase of the speed, because the increase in speed leads to an increase in the combustion rate and combustion temperature, which is favorable to $NO_x$ production. The lower temperature is beneficial to reducing NOx generation, and CO generation is mainly due to the incomplete combustion of hydrocarbons caused by local oxygen deficiency, whose main influencing factor is the mixture concentration. At medium and high speeds, the stagnation period is long and the charge factor is low, so the combustion is inadequate and intensifies the generation of CO. In terms of improving emission characteristics, Sabri Kül and Orhan [27] added CNG to diesel fuel. Compared to pure diesel fuel, the CNG blends at 500, 1250 and 2000 g/h at 100 N-m load reduced $NO_x$ emissions by 40.5, 59.4 and 68.2% (on average) and CO emissions by 8.8, 16.7 and 22.5% (average). Natural gas mixes more evenly with air in the same gas phase, so it burns more fully and therefore emits fewer emissions than gasoline.

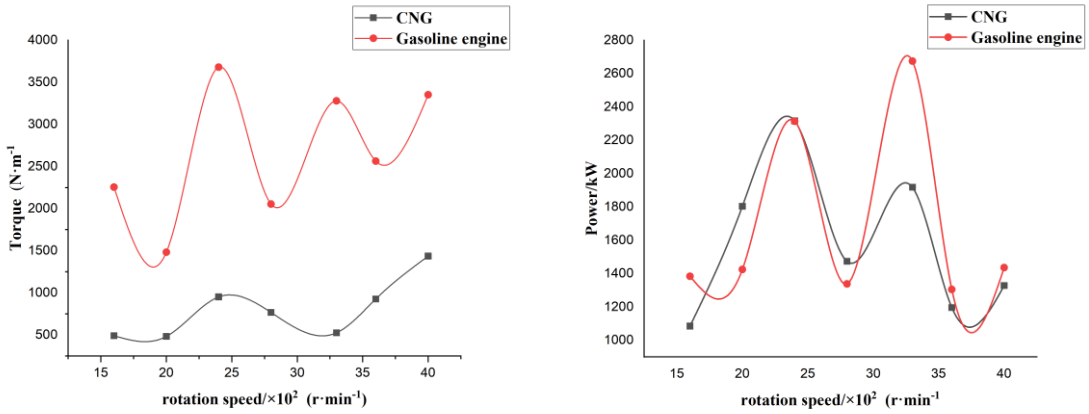


(a)Torque (b)Tower

**Figure 2.** Emission comparison of CNG internal combustion engine and gasoline engine

## CONCLUSIONS

Natural gas emits less pollutants than gasoline and is promising to solve the current serious environmental pollution problems. The following conclusions were drawn by the literature survey of the effects of combustion and emission characteristics of natural gas internal combustion engines：

(1) The power performance of natural gas engines is relatively low due to the low calorific value of the CNG combustible mixture, high ignition temperature and slow flame propagation speed. Increasing the ignition energy, at the same time properly increasing the ignition advance angle or using intake boost can improve its power performance.

(2) Compared with gasoline engines, CNG engines consume less fuel at the same power output, and injecting fuel at the optimal injection advance angle can improve the economic performance of the engine.

(3) Compared with gasoline fuel, the power performance of the engine is worse when CNG is used as fuel, the maximum difference of torque and power reaches 21.9% and 19.8%, respectively. But the emission is less, the results show that the emission of $NO_x$ is reduced by up to 81.66% and the emission of CO is reduced by up to 26.67%.

Therefore, improving the power of natural gas internal combustion engines on the basis of ensuring their emissivity is the main content of current research in this field.

## CONFLICTS OF INTEREST

The author declares that there is no conflict of interests regarding the publication of this paper.

## REFERENCES


[1] Economides, M. J. and Wood, D. A. (2009). The state of natural gas. *Journal of Natural Gas Science and Engineering*, 1(1), 1-13. DOI: https://doi.org/10.1016/j.jngse.2009.03.005.

[2] Pettifor, H., Wilson, C., Axsen, J., Abrahamse, W., and Anable, J. (2017). Social influence in the global diffusion of alternative fuel vehicles – A meta-analysis. *Journal of Transport Geography*, 62, 247-261. DOI: https://doi.org/10.1016/j.jtrangeo.2017.06.009

[3] Kontses, A., Triantafyllopoulos, G., Ntziachristos, L., and Samaras, Z. (2020). Particle number (PN) emissions from gasoline, diesel, LPG, CNG and hybrid-electric light-duty vehicles under real-world driving conditions. *Atmospheric Environment*, 222, 117126. DOI: https://doi.org/10.1016/j.atmosenv.2019.117126

[4] Yontar, A. A. and Doğu, Y. (2018). Investigation of the effects of gasoline and CNG fuels on a dual sequential ignition engine at low and high load conditions. *Fuel*, 232, 114-123. DOI: https://doi.org/10.1016/j.fuel.2018.05.156

[5] Guo, L. X., Li, C. N., Shi, D. X., Liu, Y., and Ma, L. (2019). Study on optimization of natural gas engine EGR system. *Automotive Engines*, 2019(6), 51-57.

[6] Tahir, M. M., Ali, M. S., Salim, M. A., Bakar, R. A., Fudhail, A. M., Hassan, M. Z., and Muhaimin, M. S. A. (2015). Performance Analysis of A Spark Ignition Engine Using Compressed Natural Gas (CNG) as Fuel. *Energy Procedia*, 68, 355-362. DOI: https://doi.org/10.1016/j.egypro.2015.03.266

[7] Liu, S., Su, L. W., and Tian, Y. H. (2019). Study on the improvement of air intake inhomogeneity in natural gas engines. *Automotive Engines,* 2019 (5), 41-45.

[8] Han, Z., Wu, Z., Huang, Y., Shi, Y., and Liu, W. (2021). Impact of Natural Gas Fuel Characteristics on the Design and Combustion Performance of a New Light-Duty CNG Engine. *International Journal of Automotive Technology*, 22(6), 1619-1631. DOI: 10.1007/s12239-021-0140-1

[9] Sahoo, S., and Srivastava, D. K. (2021). Effect of compression ratio on engine knock, performance, combustion and emission characteristics of a bi-fuel CNG engine. *Energy*, 233, 121144. DOI: https://doi.org/10.1016/j.energy.2021.121144

[10] Wu, W. (2021). Analysis of the current situation of China's automobile emission control level and comprehensive countermeasures. *Internal Combustion Engine and Accessories*, 2021(5), 148-149. DOI: 10.19475/j.cnki.issn1674-957x.2021.05.069

[11] Jin Y. P. (2020). Research status and development prospect of CNG application on internal combustion engine. *Modern Vehicle Power*, 2020(4), 1-5+36.

[12] Leng, X. Y., Ge, Q. Q., He, Z. X., He, D. Z. , and Long, W.Q. (2021). Combustion and emission simulation of pre-combustion chamber type natural gas doped hydrogen engine. *Journal of Internal Combustion Engines*, 2021(1), 26-33. DOI:10.16236/j.cnki.nrjxb.202101004.

[13] Wang, Y., Ma, F. H., and Liu, H. Q. (2007). Analysis of natural gas engine combustion mode. *Automotive Engines*, 2007(5), 18-21+26.

[14] Deng, J., Ma, F., Li, S., He, Y., Wang, M., Jiang, L., and Zhao, S. (2011). Experimental study on combustion and emission characteristics of a hydrogen-enriched compressed natural gas engine under idling condition. *International*

*Journal of Hydrogen Energy*, 36(20), 13150-13157. DOI: https://doi.org/10.1016/j.ijhydene.2011.07.036

[15] Yang, L.P., Song, E.Z., Ding, S.L., Brown, R. J., Marwan, N., and Ma, X.Z. (2016). Analysis of the dynamic characteristics of combustion instabilities in a pre-mixed lean-burn natural gas engine. *Applied Energy*, 183, 746-759. DOI: https://doi.org/10.1016/j.apenergy.2016.09.037

[16] Jiao, Y.J., Zhang, H.M., Si, P.K., Yang, Z.Y., Zhang, Z.L., and Cheng, H. (2009). Combustion characteristics of dilute ignition natural gas engines. *Combustion Science and Technology*, 2009(6), 541-545.

[17] Zhang, Q., Wang, X., Song, G., and Li, M. (2022). Performance and emissions of a pilot ignited direct injection natural gas engine operating at slightly premixed combustion mode. *Fuel Processing Technology*, 227, 107128. DOI: https://doi.org/10.1016/j.fuproc.2021.107128

[18] Yang, M., Lin, X. D., Xu, T., Li, D. G., Jiang, T., and Guo, L. (2019). Combustion chamber selection and its mixture formation mechanism for in-cylinder direct injection natural gas engines. *Journal of Jilin University (Engineering)*, 2019(2), 426-433. DOI:10.13229/j.cnki.jdxbgxb20180326

[19] Chauhan, B. S. and Cho, H. M. (2011). The performance and emissions analysis of a multi cylinder spark ignition engine with gasoline LPG & CNG. *Journal of the Korean Institute of Gas*, 15(4), 33-38. DOI:10.7842/kigas.2011.15.4.033

[20] Lather, R. S., and Das, L. M. (2019). Performance and emission assessment of a multi-cylinder S.I engine using CNG & HCNG as fuels. *International Journal of Hydrogen Energy*, 44(38), 21181-21192. DOI: https://doi.org/10.1016/j.ijhydene.2019.03.137

[21] Verma, S., Das, L. M., Kaushik, S. C., and Tyagi, S. K. (2019). An Experimental Comparison of Enriched Biogas and CNG on Dual Fuel Operation of a Diesel Engine. *IOP Conference Series: Earth and Environmental Science*, 264(1), 012004. DOI: 10.1088/1755-1315/264/1/012004

[22] Zheng, J., Zhou, R., Zhan, R., and Lin, H. (2022). Combustion and emission characteristics of natural gas engine with partial-catalytic oxidation of the fuel. *Fuel*, 312, 122796. DOI: https://doi.org/10.1016/j.fuel.2021.122796

[23] Hou, X.J., Lu J.Y., Zou, B., Liu, Z.E., and Cheng, C. (2020). Effect of alternative fuels on engine dynamics and emissions. *Journal of Wuhan University of Technology (Transportation Science and Engineering Edition*), 2020(3), 409-413.

[24] Sun, X. N., Zhang, H. G., Wang, X. X., Wang, D. J., Zheng, G. Y., and Sun, X. N. (2011). Effect of spark advance angle on combustion and emission characteristics of compressed natural gas engines. *Advanced Materials Research*, 383, 6085-6090. DOI:10.4028/WWW.SCIENTIFIC.NET/AMR.383-390.6085.

[25] Fan, J. M., Yang, Z. C., and Yun, H. L. (2020). Effect of compressed natural gas on the performance of internal combustion engines. *Automotive Practical Technology*, 2020 (2), 34-36. DOI:10.16638/j.cnki.1671-7988.2020.02.012

[26] Verma, G., Prasad, R. K., Agarwal, R. A., Jain, S., and Agarwal, A. K. (2016). Experimental investigations of combustion, performance and emission characteristics of a hydrogen enriched natural gas fuelled prototype spark ignition engine. *Fuel*, 178, 209-217. DOI: https://doi.org/10.1016/j.fuel.2016.03.022

[27] Sabri Kül, V., and Orhan Akansu, S. (2022). Experimental Investigation of the impact of boron nanoparticles and CNG on performance and emissions of Heavy-Duty diesel engines. *Fuel*, 324, 124470. DOI: https://doi.org/10.1016/j.fuel.2022.124470



Trends in Renewable Energy
OPEN ACCESS ISSN: 2376-2144
Peer-Reviewed Review Article futureenergysp.com/index.php/tre

# Application and Research Progress of Heat Pipe in Thermal Management of Lithium-Ion Battery

Yilin Ning*, Renyi Tao, Jiaqi Luo, and Qianchao Hu

*School of Mechanical Engineering, North China University of Water Resources and Electric Power, Zhengzhou, Henan 450045, CHINA*

Received June 20, 2022; Accepted July 17, 2022; Published August 13, 2022

Lithium-ion batteries have the advantages of high energy density, high average output voltage, long service life, and environmental protection, and are widely used in the power system of new energy vehicles. However, during the working process of the battery, the working temperature is too high or too low, which will affect the charging and discharging performance, battery capacity and battery safety. As a result, a battery thermal management system (BTMS) is essential to maintain the proper ambient temperature of the working battery. Thermal management of power batteries is a key technology to ensure maximum battery safety and efficiency. This paper discusses the significance of thermal management technology in the development of new energy vehicles, introduces the main technical means of thermal management of lithium-ion batteries for vehicle, and focuses on the current state of research on the use of various types of heat pipes in lithium-ion batteries. Finally, the use of heat pipes in the thermal control of lithium-ion batteries is promising.

*Keywords: Thermal management; Lithium-ion battery; Heat pipe; New energy vehicles*

## Introduction

Under the dual pressure of energy crisis and environmental pollution, the research and development and promotion of green and environmentally friendly new energy vehicles has become an important direction for the development of the automobile industry, in order to reduce the pressure of oil imports and automobile emissions. In order to cope with the energy crisis, electric vehicles will inevitably develop in the direction of high power, high battery life, and light weight, and the requirements for thermal management systems of automotive power batteries will also become stricter. However, insufficient attention has been paid to battery pack cooling systems and thermal management, and research activities remain limited or insufficient, both in research units and in industry. The cooling system has a certain influence on the actual specific energy of the electric vehicle. During the discharge process, the power battery pack will generate heat. Poor heat dissipation conditions can cause heat build-up and affect battery performance. If the temperature is too high, the side reaction speed of the lithium-ion battery will be accelerated, there will be potential safety hazards, and the battery capacity will be reduced. Typically, for every 15°C increase in the battery temperature, the battery life will be halved. If the temperature is too low, ion diffusion and migration can be restricted, creating dangerous side effects [1-3]. Operating at 40°C, Li-Ion batteries have been shown to last and perform almost identically to room temperature. However, when

**Corresponding author:* nyl0806@126.com

Tr Ren Energy, 2022, Vol.8, No.2, 130-144. doi: 110.17737/tre.2022.8.2.00145

the temperature is higher than 45°C, the life and performance of the battery will be greatly reduced. Ramadass et al. [4] studied the capacity attenuation of an 18650 battery after cycle charge and discharge at various ambient temperatures and found that the battery's rated capacity drops fast as the working temperature rises after many charge discharge cycles. The recommended working temperature for lithium-ion batteries is 20 to 40 °C, with a maximum temperature of 45°C. Researchers normally use 50°C as the highest limit temperature of the battery surface in their battery thermal management system research.

The heat generated by lithium-ion batteries can be attributed to a variety of factors. The Joule heat produced by the internal resistance of the battery when current flows through it and the chemical reaction heat produced by the chemical reaction in the operating process are the two main factors [5]. There is a potential of thermal runaway if the heat generated during the battery's working process is not delivered in a timely manner. This can be caused by mechanical, electrical, or thermal abuse. Mechanical abuse is usually induced by collisions that produce mechanical deformation in some batteries. Extrusion of the battery's internal diaphragm or leakage of flammable electrolyte are both possible outcomes of battery pack deformation [6]. Electrical abuse generally refers to internal short circuit and overcharge/discharge. The current is forcibly injected/discharged into/out of the battery. At this time, the current will generate heat through electrochemical reaction and accelerate, resulting in thermal runaway of the battery [7]. Heat abuse is a term used to describe localized overheating caused by differences in monomer internal resistance and heat dissipation conditions [8]. The battery will deform as a result of mechanical abuse, and the battery will deform as a result of mechanical abuse, resulting in an internal short circuit, or electrical abuse. Thermal abuse of batteries is caused by electrical abuse combined with Joule heat and chemical reaction heat. The thermal runaway chain reaction of a lithium-ion battery is triggered by heat abuse and eventually leads to thermal runaway [9]. Smoke, fire, combustion, and explosion are the most common symptoms of lithium-ion power battery accidents produced by out-of-control heat [10]. The reasons of thermal runaway are summarized in Figure 1.

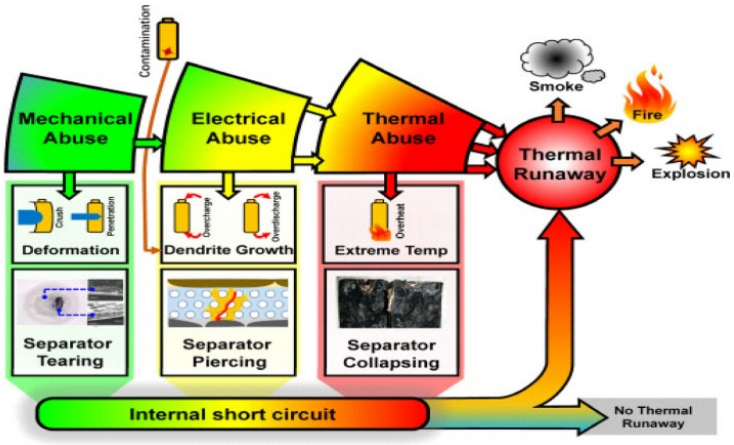


**Figure 1.** Thermal runaway caused due to rise in battery temperature [11]

**Table 1.** Electric vehicle accidents in different countries

| Date of accident | locale | Accident description | Cause of accident |
|---|---|---|---|
| 2014.1 | Japan | The power battery pack of Boeing 787 passenger plane caught fire | Thermal runaway caused by short circuit of some battery cells and defects in battery thermal management system. |
| 2015.4 | Shenzhen | Wuzhoulong pure electric bus caught fire when charging | When the battery is charged for a long time, the heat of multiple battery boxes is out of control, and the electrolyte leaks, which eventually leads to fire. |
| 2016.1 | Norway | Tesla Model s caught fire during fast charging at the super charging station | The charging algorithm has defects and can not detect the faults in the charging process. |
| 2018.5 | U.S.A | Tesla caught fire and exploded after collision | External impact |
| 2019.5 | Shanghai | Spontaneous combustion during charging of Weilai es8 | The impact caused large-area deformation of the power battery pack shell and cooling plate, resulting in short circuit of the battery. |
| 2021.4 | Guangzhou | Xiaopeng G3 spontaneous combustion during charging | Thermal runaway during charging caused by collision at the bottom of the battery box. |
| 2021.8 | U.S.A | GM bolt EV spontaneous combustion | There are two manufacturing defects in the battery: tearing of the negative pole ear and folding of the diaphragm. |

As a result, a cooling system with efficient cooling, effective preheating, and low power consumption is critical for improving electric vehicle performance and alleviating market limitations [13,14].

## Common Battery Thermal Management Technology

### Air Cooling

Air cooling is the process of using air movement to remove heat from a battery. It is separated into natural convection air cooling and forced convection air cooling depending on the driving mode. Air as a heat exchange fluid to disperse/heat the battery has become the simplest heat management approach, because it is inexpensive and easy to get, does not damage the battery, and has no effect on the electrochemical process inside the battery [15]. It is also the most popular cooling method in the research of battery heat management system [16]. The impact of improving air duct design [17], battery arrangement [18], air intake angle, air flow channel width between battery cells, and other aspects on the thermal management capabilities of the system is now the focus of research on air-cooled thermal management systems.

Zhang et al [19] developed a battery thermal management system (BTMS) based on air cooling. A transient heat transfer model was developed based on the energy equation to compute the temperature distribution of the battery pack in the BTMS. The simulated results matched the experimental results quite well. The widths of parallel channels and divergent/convergent pipes in the BTMS are developed based on the established model, which considerably increases cooling efficiency. Based on systems with varying inlet and outlet positions, Chen et al. [20] built numerous symmetrical flow channel topologies. The symmetrical system outperformed the similar asymmetric system

in terms of cooling performance. The system's maximum temperature difference was decreased by at least 43%, and its energy consumption was lowered by at least 33% after the upgrade.

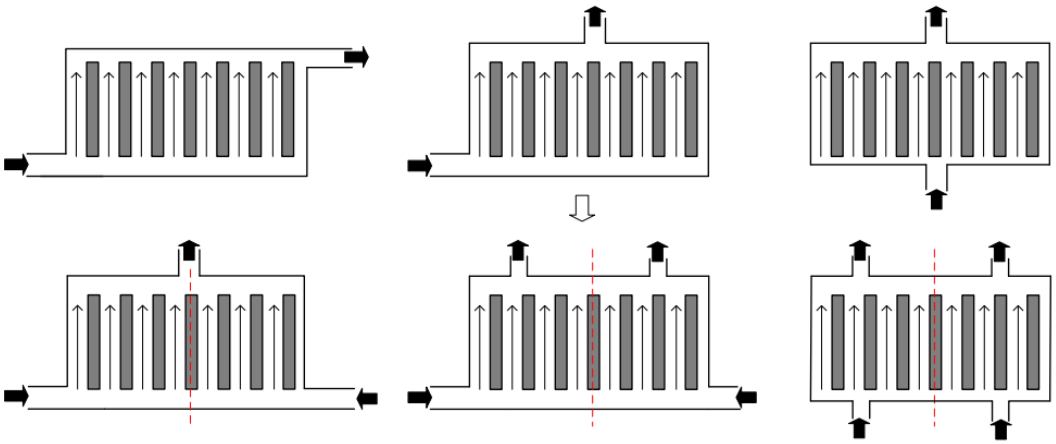

**Figure 2.** Schematics of the asymmetrical and symmetrical BTMSs [20]

## Liquid Cooling

Liquids have a greater specific heat capacity and thermal conductivity than air. Using liquids as heat exchange media to facilitate heat transfer between batteries and the external environment is an important way to improve the efficiency of thermal management systems. Direct contact and indirect contact liquid cooling are the two types of liquid cooling approaches [21]. The direct contact type usually adopts the heat exchange fluid with high heat transfer coefficient and non-conductive, such as mineral oil and ethylene glycol [22]. However, direct contact liquid cooling entails the risk of liquid leakage and requires stringent criteria for cooling medium insulation. In the non-direct contact liquid cooling system, water and antifreeze can be used as heat exchange media, but heat exchange devices such as water jackets must be used, and the liquid cooling system must be designed in conjunction with the battery pack. This results in a loss of heat exchange capacity and skyrocketing system maintenance costs, which is incompatible with the overall lightweight design of the vehicle.

The most common liquid cooling technology is the cold plate. In the cold plate, a flow channel structure is created. The heat dissipation effect is influenced by factors such as the cold plate's positioning, fluid flow velocity, temperature, and pipe configuration. Madani et al. [23] developed a cold plate-based liquid cooling system and investigated the effects of various cooling directions and pipeline distribution on the thermal performance of lithium-ion batteries. The results reveal that when the number of cooling pipes increases from four to ten, the battery's maximum temperature drops and the temperature distribution uniformity improves, but the flow pressure loss increases by 80 %. Mo et al. [24] designed a new cooling plate using topology optimization (TO) method, as shown in Figure 2. The optimized cooling plate is numerically simulated and compared with the traditional linear cooling plate. The results show that at the flow rate of $1.6\times10^{-5}$ $m^3/s$, the pressure drop and maximum temperature of the optimized cooling plate are reduced by 47.9% and 2.3℃, respectively.

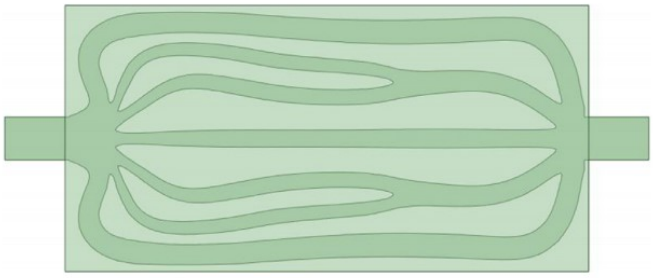

**Figure 3.** Front view of cooling plate 3D topological structure

### Phase Change Material Cooling

Cooling phase change material (PCM) does not waste system energy, but it absorbs or releases a considerable quantity of latent heat during battery pack operation to cool or heat the power battery [25]. Organic, inorganic, and composite phase change materials are the most often used PCM materials. Unlike liquid cooling, which must be paired with a channel construction, phase change cooling immerses the battery module in phase change materials, solving the problem of a small heat transfer interface in the heat dissipation design of cylindrical batteries.

Selman et al. [26] were the first to propose and patent a thermal management system based on phase change materials. They argued that using phase change materials for battery thermal management not only decreases volume but also has a greater heat dissipation effect than using convection heat dissipation. Wang et al. [27] proposed a new type of silica gel combined with PCM for BTMS. The effects of the thickness and thermal conductivity between PCM and silica gel on different cooling systems were studied. The results show that 14 mm thick PCM and 3 mm thick silica gel have the best thermal properties. Compared with the PCM cooling system without silica gel, the maximum temperature of the battery module with silica gel and PCM can be reduced by 24 ℃ at the 4 discharge rate, indicating that the BTMS can cool the battery well. In order to solve the problem of low thermal conductivity and rapid temperature increase after phase change material (PCM) completely melted, Liu et al. [28] proposed a hybrid system that couples PCM/copper foam composite with helical liquid channel cooling, the results show that the temperature drop of the hybrid system is above zero compared with natural convection. Due to the improvement of heat transfer efficiency between helical channel and PCM, helical tube can obtain lower and better battery performance than traditional liquid tube.

## Battery Thermal Management System Based on Heat Pipe

A heat pipe is a high-efficiency heat conduction element that vacuumizes a regular pipe, injects a working liquid, and then seals it. The heat pipe is separated into three sections based on its structure: condensation, insulation, and evaporation. The condensing section converts the working medium in the pipeline from gaseous state to liquid state, and also exchanges heat with the outside world, and transfers the heat in the pipeline to the outside world through the tube wall. The evaporation section exchanges heat with the heat source, receives heat from the heat source through the pipe wall and transmits it to the working medium in the pipe, and simultaneously evaporates the working medium. The adiabatic section serves two purposes: The first is to transfer heat

from the evaporation section to the condensation section via a transmission path, which is why it is also known as the transmission section. The second is to provide thermal insulation, which separates the heat source of the evaporation section from the cold source of the condensation section, allowing the heat pipe to be formed into any shape to meet the needs of working conditions. Figure 4 illustrates the heat pipe's functioning concept.

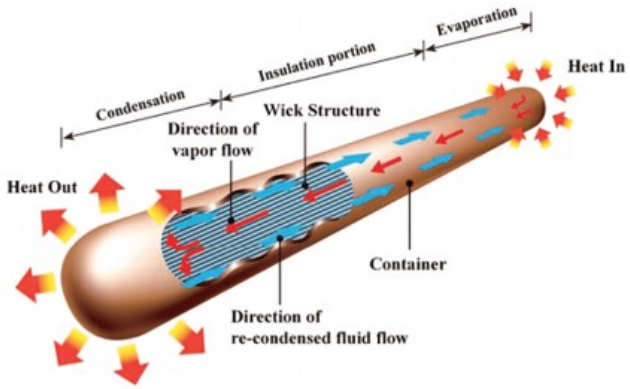


**Figure 4.** Working principle of heat pipe [29]

Heat pipe cooling was first used in the aerospace industry as a new cooling technology, with impressive results. The heat pipe cooling system for automobile power batteries is currently in the research phase. The thermal diode has good heat flow performance, is reversible, and has a high thermal conductivity [30, 31]. The high thermal conductivity of the heat pipe can quickly export the heat of the battery and realize the separation of sinks and sources at the same time. The excellent isothermal property can flatten the uneven temperature field of the battery, so as to reduce the temperature difference. The reversibility of heat flow direction can realize low-temperature preheating and high-temperature cooling of power battery. The variable heat flux and the performance of thermal diode make the control and management of heat pipe cooling system feasible [32]. Therefore, the introduction of heat pipe cooling technology into the thermal management system of power battery pack has significant advantages, feasibility and application prospects [33, 34]. The inner and outer diameters of the heat pipe, the heat pipe material, the length of each section of the heat pipe, the thermophysical parameters of the working fluid, and the liquid filling rate are all elements that affect heat transfer performance. There are currently just a few studies on the use of heat pipes as a heat dissipation method in the thermal management of electric vehicle power batteries, and the majority of the findings are still in the laboratory research stage. Scholars in the United States and overseas have conducted extensive research on the use of heat pipes in power batteries. The heat pipes used in the research mainly include gravity heat pipe [35], pulsating heat pipe, and flat plate heat pipe [36, 37].

Scholars from various countries have carried out experimental verification and simulation analysis on the application of heat pipe in power vehicle. Hussam et al. [38] investigated the heat generation and cooling of a 16-cell battery module using two distinct heat mat flat heat pipe BTMS layouts. Both structures are capable of successfully absorbing the heat generated by the battery and maintaining its temperature within the appropriate operating range. The maximum temperature difference between the battery and the heat pipe in the horizontal configuration is 6°C, and the maximum temperature difference between the battery and the heat pipe in the vertical configuration is 2°C.

Bernagozzi *et al.* [39] proposed the BTMS 3-cell battery module, which is made up of a flat ring heat pipe and graphite sheet. The loop heat pipe is placed at the module's bottom and can effectively transfer up to 150 W of heat from the battery module to the remote heat exchanger linked to the vehicle's HVAC refrigerator. Indoor experiments are used to validate the model. The results reveal that the system satisfies the battery's heat dissipation requirements. During quick charging, the highest temperature is 31.5°C, and the temperature distribution of the battery layer during an ambient temperature test is 2°C. This novel design reduces the maximum temperature after quick charging by 3.6°C when compared to the standard liquid cooling plate BTMS.

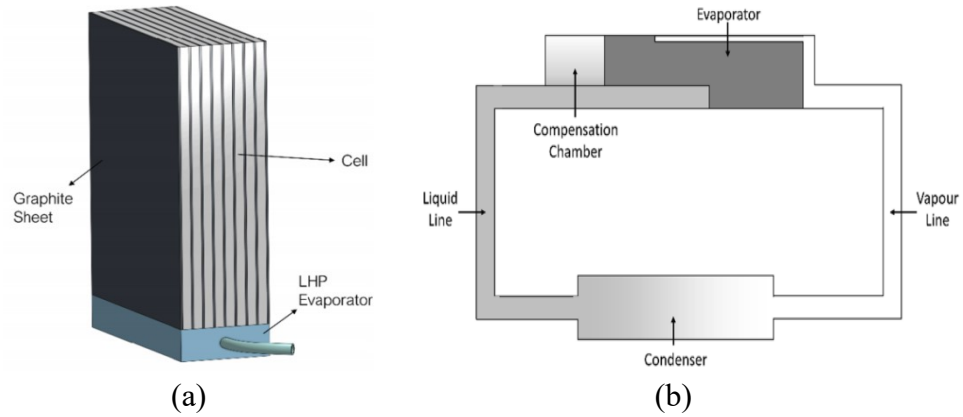


**Figure 5.** (a) Schematic diagram of coupling loop heat pipe and a single battery module. (b) Flat Plate LHP schematic.

Hussein et al. [40] designed BTMS based on heat pipe. As shown in Figure 6, the alternative battery is clamped in L-type and I-type heat pipes. The evaporation section absorbs heat from the surface of aluminum plate, and the condensation section transfers heat to the copper support. Heating was carried out at 30, 40, 50 and 60W, and the condensation section of the heat pipe was cooled with water with mass flow rates of 0.0167, 0.0333 and 0.05 kg/s, respectively. The results show that the designed BTMS based on heat pipe can make the maximum temperature ($T_{max}$) lower than 55°C even under the maximum input power, and the battery temperature difference ($\Delta T$) below 5°C.

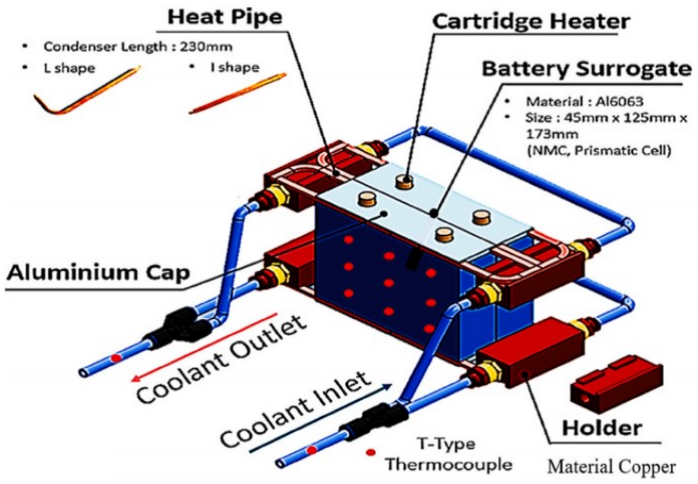


**Figure 6.** Battery BTMS based on L-shaped/I-shaped heat pipe

Chen and Li [41] applied $TiO_2$ nanofluid as working fluid in the thermal

management system of automotive lithium-ion battery of pulse heat pipe (PHP) and carried out experimental research. The structure of the experimental system is depicted in Figure 7. When the ambient temperature increases, PHP successfully prevents the maximum surface temperature of the lithium battery from increasing. The maximum temperature of the battery must not exceed 42.22°C when the ambient temperature is 35°C and the discharge rate is 1C, and the maximum temperature gradient between batteries must be less than 2°C . The technology may lower the temperature gradient and increase the thermal uniformity of the battery surface at various discharge rates.

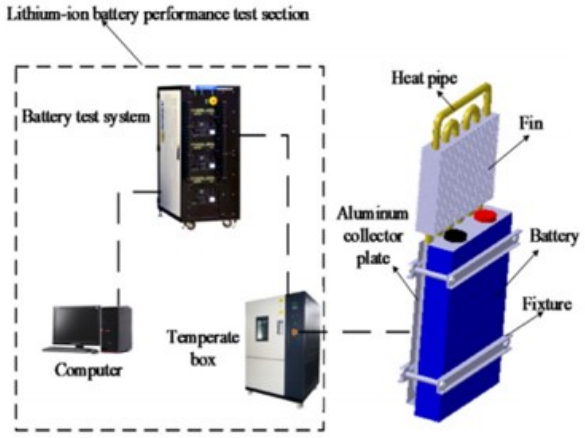


**Figure 7.** Diagram of the experimental system

Gan *et al.* [42] designed a new thermal management system based on heat pipe for cylindrical battery pack. Figure 8 depicts this BTMS. The connection between the battery and the heat pipe is made with a corrugated aluminum sleeve to maximize the heat exchange area between the heat pipe and the battery. Simultaneously, the effects of coolant flow and the length of the condenser hot pipe on the battery's temperature distribution were investigated. The findings reveal that increasing coolant flow can drastically lower the battery's maximum temperature while having no effect on temperature uniformity. The maximum temperature of the battery pack can be reduced and the temperature uniformity was improved by increasing the length of the heat pipe condensation section and the height of the corrugated aluminum sleeve.

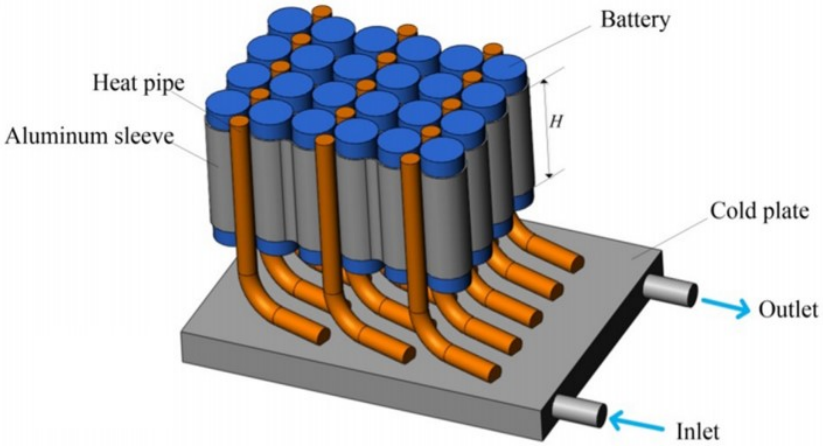


**Figure 8 .** Geometric model of battery pack and thermal management system

Wei et al. [43] explored the application of plug-in oscillating heat pipe (OHP) flat

evaporator in the electric vehicle battery thermal management. The BTMS principle based on oscillating heat pipe is shown in Figure 9. When the volume filling ratio (FRS) is 30%, 40% and 50%, considering the influence of the thermophysical properties of the working fluid on the thermal management system, the binary fluid mixture of pure water, ethanol and their different mixing ratios (MRS) (1:1 to 4:1) are used as the working medium of the heat pipe, respectively. The results show that the cooling effect is better when the ethanol water mixing ratio is 1:1. Under the input power of 56 W, the average temperature of the battery pack can be controlled below 46.5℃. In addition, the temperature uniformity of the battery module is good, and the maximum temperature difference is mostly in the range of 1-2 ℃.

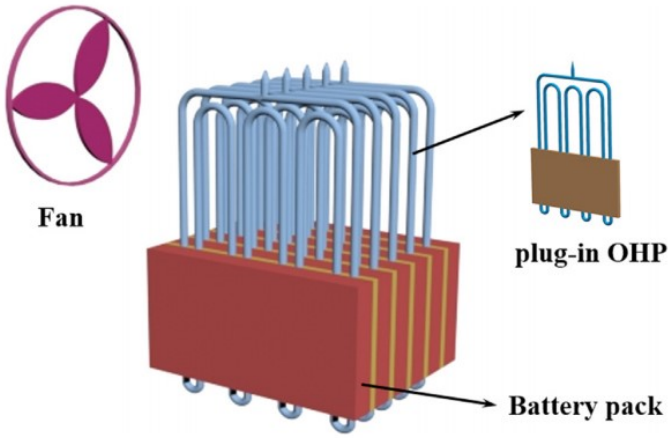


**Figure 9.** Schematic diagram of BTMS with plug-in OHPs

## BTMS with Heat Pipe Coupled with Other Cooling Methods

Dan et al. [44] devised and simulated a micro heat pipe array (MHPA) paired with forced air cooling lithium-ion battery heat management system. The heat pipe is inserted in the midst of each two square cells, the condensation section leaks out, and forced convection heat exchange with the air in the square cavity is carried out, as illustrated in Figure 10. In the transient driving situation, the thermal management system aids in limiting temperature rise and considerably improving temperature uniformity. The new heat pipe will only increase the thermal management system's overall quality by around 6.5 %, but it will significantly improve the battery pack's thermal performance.

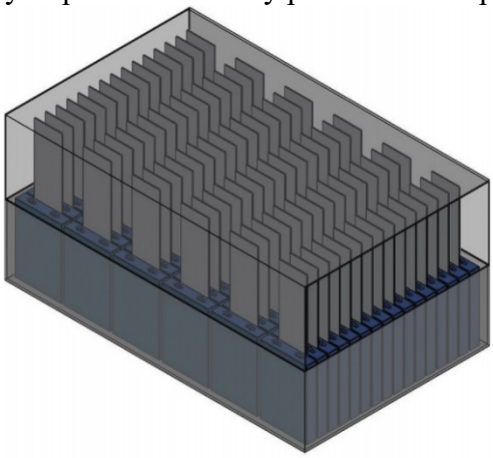

**Figure 10.** Schematic diagram of the MHPA thermal management system

Chen et al. [45] studied the effect of heat pipe on the temperature distribution in the battery pack by experimental method. The research shows that the PCM heat pipe coupling system has a positive cooling effect on the battery pack, which can basically ensure the operation of the battery in the optimal temperature range. Compared with the pure PCM system, the use of heat pipe can reduce the temperature rise of the battery by 10 ℃. Jiang et al. [46] established a lumped heat model considering the coupling of battery heat generation, phase change material melting and heat pipe transient thermal response. The coupling mechanism between battery temperature and phase change process under different ambient temperature, condensation cross-section heat transfer coefficient and thickness ratio of phase change material to battery is revealed. Chen et al. [47] conducted numerical research on the battery thermal management system (BTMS) coupled with phase change material (PCM) and heat pipe (HP). Fig. 11 is the structural diagram of the coupling system. Comparing the BTMS performance of phase change material and heat pipe coupling with that of heat pipe alone, it is found that the coupling system can reduce the temperature difference of battery pack more effectively. Under the condition of ensuring economy, the optimal design of PCM thickness is proposed. After optimization, the maximum temperature difference of battery pack is reduced by about 30%.

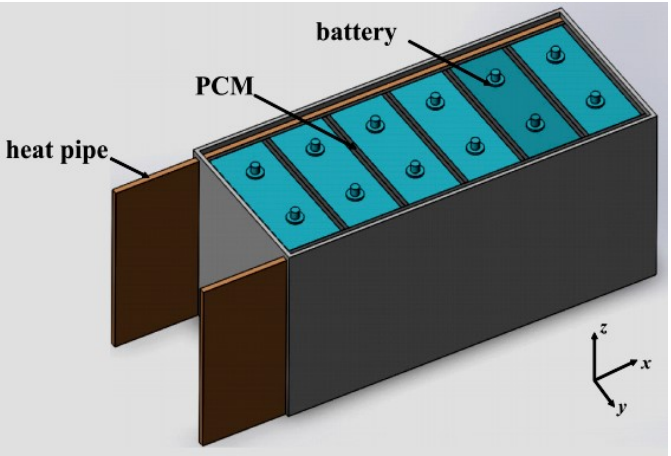


**Fig 11.** Schematic of the designed BTMS

In addition to the traditional design of heat pipe diameter, length of each section, wick and heat pipe materials, more and more people focus on the working fluid of heat pipe. Nanofluid has good thermal conductivity and phase change characteristics. Adding nano-materials to the base liquid can not only improve the thermal conductivity of the base liquid and reduce the undercooling, but also improve the specific heat capacity and the heat transfer performance of the solution [48]. Shuoman et al. [49] applied alumina nanofluid to thermosyphon, carried out experimental and theoretical research on its thermal properties, and analyzed different methods of using nano materials and their influence on improving the efficiency of BTMS. The results fully confirmed the superiority of nanofluids in improving the performance of heat pipes.

## CONCLUSIONS

According to different heat production laws of batteries, different types of heat pipes are selected and designed to meet the needs of battery heat dissipation. The use of a heat pipe in a lithium-ion battery's thermal management system increases the uniformity of temperature distribution and effectively limits the battery's maximum temperature. The heat pipe's working concept and structure are basic, and it's simple to combine with different cooling systems. While increasing the battery's efficiency and safety, it has no effect on the heat management system's overall lightweight design. The battery thermal management system based on heat pipe has emerged as a major study focus for researchers both at home and abroad, yielding numerous scientific findings with application potential.

## CONFLICTS OF INTEREST

The authors declare that there is no conflict of interests regarding the publication of this paper.

## REFERENCES

[1] Jaguemont, J., Boulon, L., and Dubé, Y. (2016). A comprehensive review of lithium-ion batteries used in hybrid and electric vehicles at cold temperatures. *Applied Energy*, 164, 99-114. DOI: https://doi.org/10.1016/j.apenergy.2015.11.034
[2] Bodenes, L., Naturel, R., Martinez, H., Dedryvère, R., Menetrier, M., Croguennec, L., Pérès, J.-P., Tessier, C., and Fischer, F. (2013). Lithium secondary batteries working at very high temperature: Capacity fade and understanding of aging mechanisms. *Journal of Power Sources*, 236, 265-275. DOI: https://doi.org/10.1016/j.jpowsour.2013.02.067
[3] Liu, H., Wei, Z., He, W., and Zhao, J. (2017). Thermal issues about Li-ion batteries and recent progress in battery thermal management systems: A review. *Energy Conversion and Management*, 150, 304-330. DOI: https://doi.org/10.1016/j.enconman.2017.08.016
[4] Ramadass, P., Haran, B., White, R., and Popov, B. N. (2002). Capacity fade of Sony 18650 cells cycled at elevated temperatures: Part I. Cycling performance. *Journal of Power Sources*, 112(2), 606-613. DOI: https://doi.org/10.1016/S0378-7753(02)00474-3
[5] Wen, J., Yu, Y., and Chen, C. (2012). A Review on Lithium-Ion Batteries Safety Issues: Existing Problems and Possible Solutions. *Materials Express*, 2(3), 197-212. DOI: 10.1166/mex.2012.1075
[6] Zhang, S., Zhou, Q., and Xia, Y. (2015). *Influence of mass distribution of battery and occupant on crash response of small lightweight electric vehicle* (No. 2015-01-0575). SAE Technical Paper. DOI: https://doi.org/10.4271/2015-01-0575
[7] Karulkar, M., Steele, L. A. M., Lamb, J., Orendorff, C. J., and Torres-Castro, L. (2018). High Precision Characterization of Lithium Plating and Abuse Response during Extreme Fast Charge (XFC) of Lithium Ion Batteries. *ECS Meeting Abstracts*, MA2018-01(1), 122-122. DOI: 10.1149/ma2018-01/1/122

[8] Wang, Y., Gao, Q., Wang, G., Zhang, T., and Yuan, M. Simulation of mixed inner air-flow integrated thermal management with temperature uniformity of Li-ion battery. *Journal of Jilin University (Engineering and Technology Edition)*, 48(5), 1339-1348. DOI: 10.13229/j.cnki.jdxbgxb20170860
[9] Greve, L., and Fehrenbach, C. (2012). Mechanical testing and macro-mechanical finite element simulation of the deformation, fracture, and short circuit initiation of cylindrical Lithium ion battery cells. *Journal of Power Sources*, 214, 377-385. DOI: https://doi.org/10.1016/j.jpowsour.2012.04.055
[10] Wang, Q., Ping, P., Zhao, X., Chu, G., Sun, J., and Chen, C. (2012). Thermal runaway caused fire and explosion of lithium ion battery. *Journal of Power Sources*, 208, 210-224. DOI: https://doi.org/10.1016/j.jpowsour.2012.02.038
[11] Azizi, Y., and Sadrameli, S. M. (2016). Thermal management of a LiFePO4 battery pack at high temperature environment using a composite of phase change materials and aluminum wire mesh plates. *Energy Conversion and Management*, 128, 294-302. DOI: https://doi.org/10.1016/j.enconman.2016.09.081
[12] Ji, Y., and Wang, C. Y. (2013). Heating strategies for Li-ion batteries operated from subzero temperatures. *Electrochimica Acta*, 107, 664-674. DOI: https://doi.org/10.1016/j.electacta.2013.03.147
[13] Pesaran, A., Santhanagopalan, S.,and Kim, G. H. (2013). *Addressing the Impact of Temperature Extremes on Large Format Li-Ion Batteries for Vehicle Applications (Presentation)*. United States.
[14] Gao, Q., Liu, Y., Wang, G., Deng, F., and Zhu, J. (2019). An experimental investigation of refrigerant emergency spray on cooling and oxygen suppression for overheating power battery. *Journal of Power Sources*, 415, 33-43. DOI: https://doi.org/10.1016/j.jpowsour.2019.01.052
[15] Chen, K., Chen, Y., Li, Z., Yuan, F., and Wang, S. (2018). Design of the cell spacings of battery pack in parallel air-cooled battery thermal management system. *International Journal of Heat and Mass Transfer*, 127, 393-401. DOI: https://doi.org/10.1016/j.ijheatmasstransfer.2018.06.131
[16] Hong, S., Zhang, X., Chen, K., and Wang, S. (2018). Design of flow configuration for parallel air-cooled battery thermal management system with secondary vent. *International Journal of Heat and Mass Transfer*, 116, 1204-1212. DOI: https://doi.org/10.1016/j.ijheatmasstransfer.2017.09.092
[17] Saw, L. H., Ye, Y., Tay, A. A. O., Chong, W. T., Kuan, S. H., and Yew, M. C. (2016). Computational fluid dynamic and thermal analysis of Lithium-ion battery pack with air cooling. *Applied Energy*, 177, 783-792. DOI: https://doi.org/10.1016/j.apenergy.2016.05.122
[18] Yang, N., Zhang, X., Li, G., and Hua, D. (2015). Assessment of the forced air-cooling performance for cylindrical lithium-ion battery packs: A comparative analysis between aligned and staggered cell arrangements. *Applied Thermal Engineering*, 80, 55-65. DOI: https://doi.org/10.1016/j.applthermaleng.2015.01.049
[19] Zhang, J., Wu, X., Chen, K., Zhou, D., and Song, M. (2021). Experimental and numerical studies on an efficient transient heat transfer model for air-cooled battery thermal management systems. *Journal of Power Sources*, 490, 229539. DOI: https://doi.org/10.1016/j.jpowsour.2021.229539
[20] Chen, K., Chen, Y., She, Y., Song, M., Wang, S., and Chen, L. (2020). Construction of effective symmetrical air-cooled system for battery thermal management. *Applied Thermal Engineering*, 166, 114679. DOI:

https://doi.org/10.1016/j.applthermaleng.2019.114679
[21] Madani, S. S., Swierczynski, M. J., and Kær, S. K. A review of thermal management and safety for lithium ion batteries. In: *Proc., 2017 Twelfth International Conference on Ecological Vehicles and Renewable Energies (EVER)*, pp: 1-20. DOI: 10.1109/EVER.2017.7935914
[22] Mondal, B., Lopez, C. F., and Mukherjee, P. P. (2017). Exploring the efficacy of nanofluids for lithium-ion battery thermal management. *International Journal of Heat and Mass Transfer*, 112, 779-794. DOI: https://doi.org/10.1016/j.ijheatmasstransfer.2017.04.130
[23] Madani, S. S., Schaltz, E., and Kær, S. K. (2020). Thermal Analysis of Cold Plate with Different Configurations for Thermal Management of a Lithium-Ion Battery. 6(1), 17. DOI: https://doi.org/10.3390/batteries6010017
[24] Mo, X., Zhi, H., Xiao, Y., Hua, H., and He, L. (2021). Topology optimization of cooling plates for battery thermal management. *International Journal of Heat and Mass Transfer*, 178, 121612. DOI: https://doi.org/10.1016/j.ijheatmasstransfer.2021.121612
[25] Lazrak, A., Fourmigué, J.-F., and Robin, J.-F. (2018). An innovative practical battery thermal management system based on phase change materials: Numerical and experimental investigations. *Applied Thermal Engineering*, 128, 20-32. DOI: https://doi.org/10.1016/j.applthermaleng.2017.08.172
[26] Khateeb, S. A., Farid, M. M., Selman, J. R., and Al-Hallaj, S. (2004). Design and simulation of a lithium-ion battery with a phase change material thermal management system for an electric scooter. *Journal of Power Sources*, 128(2), 292-307. DOI: https://doi.org/10.1016/j.jpowsour.2003.09.070
[27] Wang, J., Huang, Q., Li, X., Zhang, G., and Wang, C. (2021). Experimental and numerical simulation investigation on the battery thermal management performance using silicone coupled with phase change material. *Journal of Energy Storage*, 40, 102810. DOI: https://doi.org/10.1016/j.est.2021.102810
[28] Liu, H., Ahmad, S., Shi, Y., and Zhao, J. (2021). A parametric study of a hybrid battery thermal management system that couples PCM/copper foam composite with helical liquid channel cooling. *Energy*, 231, 120869. DOI: https://doi.org/10.1016/j.energy.2021.120869
[29] Huang, Y., Tang, Y., Yuan, W., Fang, G., Yang, Y., Zhang, X., Wu, Y., Yuan, Y., Wang, C., and Li, J. (2021). Challenges and recent progress in thermal management with heat pipes for lithium-ion power batteries in electric vehicles. *Science China Technological Sciences*, 64(5), 919-956. DOI: 10.1007/s11431-020-1714-1
[30] Gao, X., Wu, W., Meng, Z., Liu, P., Zhao, W., and Wang, X. (2017). Thermal performance of solar collector with energy storage materials and oscillating heat pipe. *Transactions of the Chinese Society of Agricultural Engineering*, 33(16), 234-240.
[31] He, L., Tang, X., Luo, Q., Liao, Y., Luo, X., Liu, J., Ma, L., Dong, D., Gan, Y., and Li, Y. (2022). Structure optimization of a heat pipe-cooling battery thermal management system based on fuzzy grey relational analysis. *International Journal of Heat and Mass Transfer*, 182, 121924. DOI: https://doi.org/10.1016/j.ijheatmasstransfer.2021.121924
[32] Liang, J., Gan, Y., and Li, Y. (2018). Investigation on the thermal performance of a battery thermal management system using heat pipe under different ambient temperatures. *Energy Conversion and Management*, 155, 1-9. DOI: https://doi.org/10.1016/j.enconman.2017.10.063
[33] Liang, L., Zhao, Y., Diao, Y., Ren, R., and Jing, H. (2021). Inclined U-shaped flat microheat pipe array configuration for cooling and heating lithium-ion battery modules in

electric vehicles. *Energy*, 235, 121433. DOI: https://doi.org/10.1016/j.energy.2021.121433
[34] Mbulu, H., Laoonual, Y., and Wongwises, S. (2021). Experimental study on the thermal performance of a battery thermal management system using heat pipes. *Case Studies in Thermal Engineering*, 26, 101029. DOI: https://doi.org/10.1016/j.csite.2021.101029
[35] Yang, S., Ling, C., Fan, Y., Yang, Y., Tan, X., and Dong, H. (2019). A review of lithium-ion battery thermal management system strategies and the evaluate criteria. *International Journal of Electrochemical Science*, *14*(7), 6077-6107.
[36] Zhao, J., Rao, Z., Liu, C., and Li, Y. (2016). Experiment study of oscillating heat pipe and phase change materials coupled for thermal energy storage and thermal management. *International Journal of Heat and Mass Transfer*, 99, 252-260. DOI: https://doi.org/10.1016/j.ijheatmasstransfer.2016.03.108
[37] Chi, R.-G., Chung, W.-S., and Rhi, S.-H. (2018). Thermal Characteristics of an Oscillating Heat Pipe Cooling System for Electric Vehicle Li-Ion Batteries. 11(3), 655. DOI: https://doi.org/10.3390/en11030655
[38] Jouhara, H., Delpech, B., Bennett, R., Chauhan, A., Khordehgah, N., Serey, N., and Lester, S. P. (2021). Heat pipe based battery thermal management: Evaluating the potential of two novel battery pack integrations. *International Journal of Thermofluids*, 12, 100115. DOI: https://doi.org/10.1016/j.ijft.2021.100115
[39] Bernagozzi, M., Georgoulas, A., Miché, N., Rouaud, C., and Marengo, M. (2021). Novel battery thermal management system for electric vehicles with a loop heat pipe and graphite sheet inserts. *Applied Thermal Engineering*, 194, 117061. DOI: https://doi.org/10.1016/j.applthermaleng.2021.117061
[40] Mbulu, H., Laoonual, Y., and Wongwises, S. (2021). Experimental study on the thermal performance of a battery thermal management system using heat pipes. *Case Studies in Thermal Engineering*, 26, 101029. DOI: https://doi.org/10.1016/j.csite.2021.101029
[41] Chen, M., and Li, J. (2020). Nanofluid-based pulsating heat pipe for thermal management of lithium-ion batteries for electric vehicles. *Journal of Energy Storage*, 32, 101715. DOI: https://doi.org/10.1016/j.est.2020.101715
[42] Gan, Y., He, L., Liang, J., Tan, M., Xiong, T., and Li, Y. (2020). A numerical study on the performance of a thermal management system for a battery pack with cylindrical cells based on heat pipes. *Applied Thermal Engineering*, 179, 115740. DOI: https://doi.org/10.1016/j.applthermaleng.2020.115740
[43] Wei, A., Qu, J., Qiu, H., Wang, C., and Cao, G. (2019). Heat transfer characteristics of plug-in oscillating heat pipe with binary-fluid mixtures for electric vehicle battery thermal management. *International Journal of Heat and Mass Transfer*, 135, 746-760. DOI: https://doi.org/10.1016/j.ijheatmasstransfer.2019.02.021
[44] Dan, D., Yao, C., Zhang, Y., Zhang, H., Zeng, Z., and Xu, X. (2019). Dynamic thermal behavior of micro heat pipe array-air cooling battery thermal management system based on thermal network model. *Applied Thermal Engineering*, 162, 114183. DOI: https://doi.org/10.1016/j.applthermaleng.2019.114183
[45] Chen, H. B., Cao, H. Z., Li, H. X., Zhao, X. W., and Liu, X. F. Experimental Study on Coupled Cooling System of PCM-Heat Pipe for Vehicle Power Battery Pack. In: *Proc., Proceedings of the 2015 International Conference on Electrical, Automation and Mechanical Engineering*, Atlantis Press, pp: 448-451. DOI: https://doi.org/10.2991/eame-15.2015.127

[46] Jiang, Z. Y., and Qu, Z. G. (2019). Lithium–ion battery thermal management using heat pipe and phase change material during discharge–charge cycle: A comprehensive numerical study. *Applied Energy*, 242, 378-392. DOI: https://doi.org/10.1016/j.apenergy.2019.03.043
[47] Chen, K., Hou, J., Song, M., Wang, S., Wu, W., and Zhang, Y. (2021). Design of battery thermal management system based on phase change material and heat pipe. *Applied Thermal Engineering*, 188, 116665. DOI: https://doi.org/10.1016/j.applthermaleng.2021.116665
[48] Nazari, M. A., Ahmadi, M. H., Sadeghzadeh, M., Shafii, M. B., and Goodarzi, M. (2019). A review on application of nanofluid in various types of heat pipes. *Journal of Central South University*, 26(5), 1021-1041. DOI: 10.1007/s11771-019-4068-9
[49] Shuoman, L. A., Abdelaziz, M., and Abdel-Samad, S. (2021). Thermal performances and characteristics of thermosyphon heat pipe using alumina nanofluids. *Heat and Mass Transfer*, 57(8), 1275-1287. DOI: 10.1007/s00231-021-03031-y



# CALL FOR PAPERS

# Trends in Renewable Energy

**ISSN Print: 2376-2136 ISSN online: 2376-2144**

**http://futureenergysp.com/index.php/tre/**

Trends in Renewable Energy (TRE) is an open accessed, peer-reviewed semi-annual journal publishing reviews and research papers in the field of renewable energy technology and science. The aim of this journal is to provide a communication platform that is run exclusively by scientists. This journal publishes original papers including but not limited to the following fields:

- ✧ Renewable energy technologies
- ✧ Catalysis for energy generation, Green chemistry, Green energy
- ✧ Bioenergy: Biofuel, Biomass, Biorefinery, Bioprocessing, Feedstock utilization, Biological waste treatment,
- ✧ Energy issues: Energy conservation, Energy delivery, Energy resources, Energy storage, Energy transformation, Smart Grid
- ✧ Environmental issues: Environmental impacts, Pollution
- ✧ Bioproducts
- ✧ Policy, etc.

We publish the following article types: peer-reviewed reviews, mini-reviews, technical notes, short-form research papers, and original research papers.

*The article processing charge (APC), also known as a publication fee, is fully waived for the Trends in Renewable Energy.*

## Call for Editorial Board Members

We are seeking scholars active in a field of renewable energy interested in serving as volunteer Editorial Board Members.

**Qualifications**

Ph.D. degree in related areas, or Master's degree with a minimum of 5 years of experience. All members must have a strong record of publications or other proofs to show activities in the energy related field.

If you are interested in serving on the editorial board, please email CV to editor@futureenergysp.com.